Engineering Structures 257 (2022) 114077

Contents lists available at ScienceDirect

Engineering Structures

journal homepage: www.elsevier.com/locate/engstruct

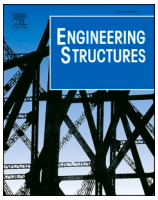

# Fragility curves for different classes of existing RC buildings under ground differential settlements

Andrea Miano *, Annalisa Mele, Andrea Prota

*Department of Structures for Engineering and Architecture, University of Naples Federico II, Italy*

ARTICLE INFO

*Keywords:*
Existing RC buildings
Fragility curves
Latin Hypercube Sampling
Differential settlements
Incremental Analysis
SAP-Matlab integration
OAPI

ABSTRACT

Existing reinforced concrete (RC) buildings can be affected by different actions that can induce permanent or transient effects on them. While applications concerning the seismic vulnerability of existing RC buildings have been largely proposed in literature, the evaluation of the structural vulnerability because of hazards different from earthquake has been less dealt with. The focus of this work is to estimate the probability that the simulated RC buildings stock could reach a given Limit State for a certain intensity of imposed monotonically increasing ground differential settlements. A set of simulated FEM models, considering the geometrical and mechanical uncertainties in the representation of the existing RC frame buildings designed only for gravitational loads, has been created. The structural frames differ from each other for geometrical features and mechanical materials properties, obtained through a simulation process. The non-linear behavior of columns and beams is considered by applying a modeling approach specifically elaborated for RC members with plain bars. A FEM model for each simulated structural frame has been developed using the Open Application Programming Interface by using the programming and numeric computing platform MATLAB to run the modelling software SAP2000. Time by time, by scaling up the amplitude of the imposed base displacements, a non-linear static incremental procedure has been implemented. At each step of the analysis, a code-based seismic safety assessment has been carried out with reference to a specific ultimate Limit State considered in the Italian and European codes. The goal of the analysis has been to find the values of the significative structural response parameters (identified in this work as the maximum differential settlement and the deflection ratio) at the onset of the selected Limit State by using the critical demand to capacity ratio. Considering that these values are lognormally distributed, the structural fragility is then derived, showing how the vulnerability of the considered RC buildings stock is affected by the impact of the geometrical features and by the application direction of the differential settlements.

## 1. Introduction

Existing structures can be affected by different hazard sources (e.g., monotonically acting, such as the landslides or the subsidence, or cyclic, such as the earthquakes) that can induce permanent or transient effects on them. With respect to the seismic vulnerability analysis of existing reinforced concrete (RC) buildings, many methodologies and applications have been presented with the scope of defining fragility curves based on different modeling strategy and analysis methodology [1–4] and under the consideration of the different sources of uncertainties in the modeling phase [5–7]. The evaluation of the vulnerability of existing RC buildings as consequence of hazards different from earthquake, instead, is a poorly approached theme in literature. The focus of this work is to evaluate the vulnerability of a selected RC buildings stock designed only for gravitational loads, when monotonically increasing differential settlements, that may be induced by non-cyclical hazard sources – e.g., landslides, subsidence, anthropic causes – are applied at the columns basis.

The literature about the correlation among differential foundation settlements and damage assessment is quite variegate, but mainly related to empirical relations. Recommendations on allowable settlements, selecting as damage criterion the angular distortion (defined as the rotation of the straight line joining two reference points on the structure, minus any rigid body tilt of the structure) or the deflection ratio (defined as the maximum displacement of the settlement profile relative to the straight line connecting two settlement reference points, divided by the distance between the two reference points), were provided from Skempton and MacDonald [8] and Bjerrum [9] mainly for

* Corresponding author.
*E-mail address:* andrea.miano@unina.it (A. Miano).

https://doi.org/10.1016/j.engstruct.2022.114077
Received 12 November 2021; Received in revised form 13 January 2022; Accepted 26 February 2022

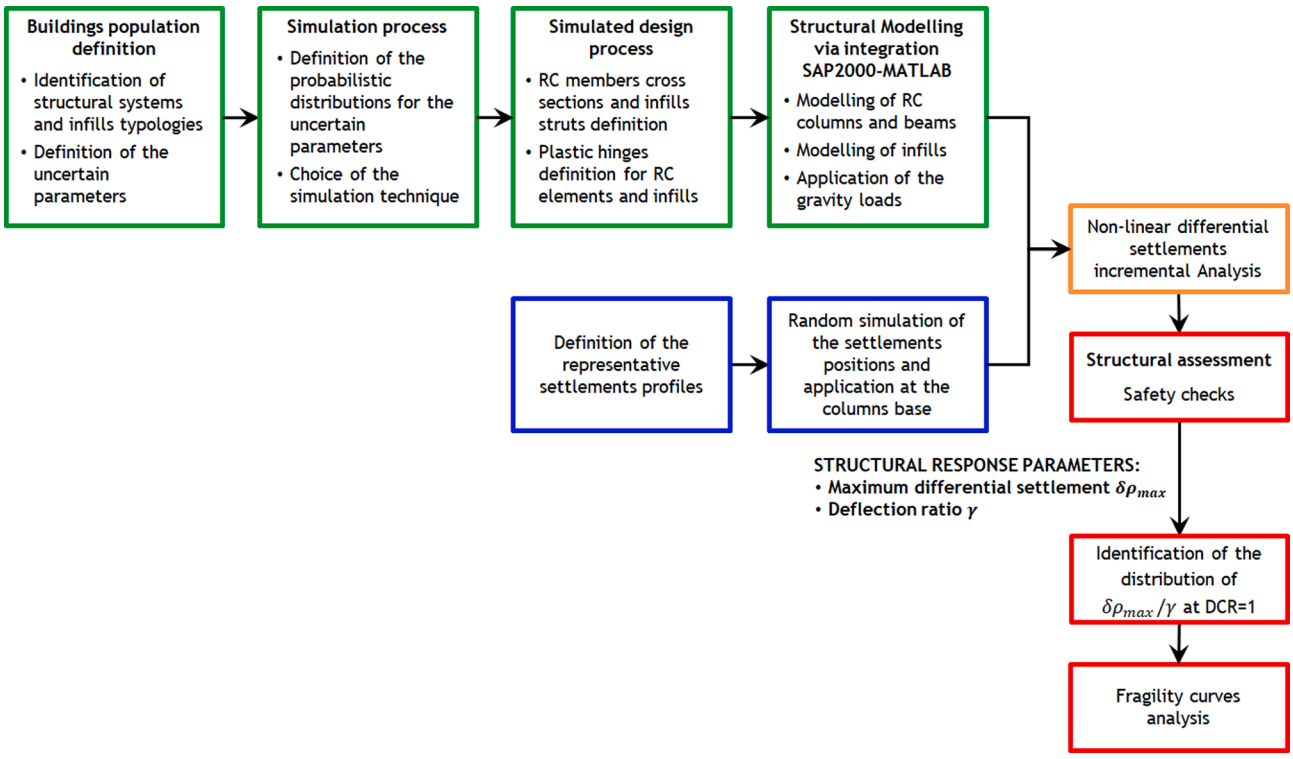


**Fig. 1.** Flowchart of the proposed procedure.

infilled steel and RC frame structures, from Meyerhof [10] for framed panels and loadbearing brick walls, from Polshin and Tokar [11] for frame structures and continuous load bearing structures. Burland and Wroth [12] linked the onset of the visible cracking with a critical tensile strain, proposing as engineering demand parameter also the deflection ratio. Burland et al. [13] presented a classification of 5 points of visible or aesthetic damage to walls, correlated to the maximum expected settlement/angular distortion. Boscardin and Cording [14] included the effect of horizontal strain developing in the ground due to settlements, and defined damage categories by relating the horizontal strain and the angular distortion. Boone [15] proposed a Strain Superposition Method to evaluate the building damage by considering ground deformation patterns, damage category criteria and strain concept. The described engineering demand parameters were used in the following years, associating them to damage thresholds for the different structural typologies. The different limitations about the damage thresholds are summarized in Poulos et al. [16], as function of the type of structure and the type of damage/concern. Instead, with respect to mechanical approaches, Finno et al. [17] presented a semi-empirical laminated beam method to evaluate potential building damage due to excavation-induced ground movements, that avoids the common over-simplification of the empirical methods, even not to be considerable as a detailed finite element analysis. In fact, it is assumed that the floors offer restraint to bending deformations, and the walls offer restraint to shear deformations. Negulescu and Foerster [18] presented a parametric analysis to build analytical fragility curves, which express the probability of achieving a given damage state of the structure as function of the differential displacements. Fotopoulou et al. [19] proposed a numerical methodology for the performance-based vulnerability assessment of typical RC frame buildings subjected to liquefaction-induced differential ground displacements, and Gomez-Martinez et al. [20] estimated the potential relevance of differential settlements in the earthquake-induced liquefaction damage assessment. Moreover, Bao et al. [21], examined the influence of differential settlement on the seismic performance of a steel moment resisting frame structure through a nonlinear time-history analysis followed by IDA and seismic fragility analysis.

In recent years, many applications have investigated the effects of ground deformations displacements induced by landslides [22–23] or different hazard sources, such as subsidence [24], ground consolidation [25], mining activities [26], excavations [27] by using satellite data. These hazard sources, inducing quite slow-in-time displacements under the existing buildings, can be monitored both through traditional techniques and more innovative remote sensing techniques, exploiting satellite data [28]. Then, the proposed vulnerability assessment analysis can be easily combined with the remote sensing data to perform structural evaluation for existing RC buildings. For example, Nappo et al. [29] developed fragility curves for existing buildings, by investigated the empirical correlation between the subsidence, monitored with satellite data in terms of differential settlements and relative rotations, and damage in the buildings.

The focus of this work is to evaluate the vulnerability of a selected RC buildings stock, subdivided as function of the geometrical features (*number of floors* and *span length*), in order to define the probability of reaching a given Limit State (*ls*) for a certain intensity of the hazard *maximum differential settlement* and *deflection ratio*. The considered buildings stock is designed only for gravitational loads, typically having a structural setting consisting in parallel plane frames. A RC infilled buildings' population is simulated, identifying the uncertain parameters related to geometrical and mechanical materials properties and finalizing the structural design of the elements through a simulated design procedure. For each case study building, the focus is concentrated on an external plane frame. A novelty of the work consists in the creation of the FEM model of each simulated case study structural frame, using the *Open Application Programming Interface* (OAPI) by CSI [30], that allows the integrated use between the FEM software SAP2000 [30] and the programming and numeric computing platform MATLAB [31]. The non-linear behavior of the structural RC members is considered by applying a modeling approach specifically elaborated for RC members with plain bars [32]. Infills are modeled as a couple of diagonal struts resisting only to compression, with mechanical characteristics defined as indicated by [33]. Then, time by time, a non-linear static incremental procedure is

implemented, by scaling up the amplitude of the imposed base displacements, obtained by the simulation operation. The applied procedure is conceptually identical to the Incremental Dynamic Analysis [34], very well known in literature for seismic applications (e.g., [35–37]). At each step of the analysis, a code-based seismic safety assessment is carried out with reference to an ultimate *ls* condition, accordingly to the Italian National Code [38] and to the Eurocode 8 – Part 3 [39]. The significative structural response parameters identified in this work are the *maximum differential settlement* and the *maximum deflection ratio*, referred to each segment of the profile. The goal of the analysis is to find the values of these parameters at the onset of the selected *ls*, by using the critical demand to capacity ratio [40–41]. Considering that these values are lognormally distributed, the structural fragility is then derived [40,42].

This work demonstrates that the geometrical parameters of the considered RC frames stock have a significant impact on the frame vulnerability measure, when subjected to base differential displacements. Moreover, the application direction of the differential settlements induces a clear differentiation in the vulnerability response among the analyzed RC frames, when the selected geometrical parameter varies.

## 2. Methodology

The methodology proposed in this work is summarized in the flowchart in Fig. 1. The first step of the proposed methodology is the identification of the buildings' population. Once the structural type is defined, the uncertain parameters related to geometry and material mechanical properties are identified through a literature study of the main characteristics of the existing RC buildings in Italy and, more in general, of the Mediterranean area. Then, the structural models are obtained, by simulating the uncertain parameters. Subsequently, based on each simulated suite of parameters, different structural frames are set. For each one, the RC members' cross sections are obtained by means of a simulated design process, and, with the aim of performing a non-linear analysis, the plastic hinges for RC elements and infills are defined. The following step is the structural modelling via the integration between SAP2000 and MATLAB. At this point, after defining the representative settlement profiles and simulating their position under the columns of each frame, the displacements are imposed in the models. Non-linear differential settlements incremental analyses are then implemented, by scaling up the amplitude of the base displacements. A structural assessment is done at each step of the incremental analysis, by considering all the possible failure mechanisms. Once the structural response parameter is identified – in this work the *maximum differential settlement* along the profile or the *maximum deflection ratio* referred to each segment of the profile – the goal of the analysis is to find the values of this parameter at the onset of the selected *ls*. Considering that these values are lognormally distributed, the structural fragility is then derived. In Section 2.1 the simulation process is examined, while in Section 2.2 the structural assessment is presented. Finally, in Section 2.3 the derivation of the fragility curves is illustrated.

### 2.1. Simulation process

This Section describes the adopted simulation process. The choice of the sampling technique to simulate the uncertain structural model parameters is the fundamental step in the definition of the proposed methodology. The Latin Hypercube Sampling (LHS, [43]) is used in this work. It is a special type of MonteCarlo simulation (MCS, [44]), which uses the stratification of the theoretical probability distribution functions of input random variables. LHS can be considered as an alternative to the crude MCS in order to reduce the number of simulations and saving computational time [45] in addition to gaining acceptable level of accuracy (e.g., reducing the variance of the response function compared to the crude MCS, [46]). In this work, an efficient technique to carry out sample selection in LHS, which is the sampling of interval mean values (see a complete discussion in [47]), is chosen. The sampling from each interval is implemented only once during the simulation. The realizations of LHS are then completed by randomly pairing up the resulting values for each of the random variables [7,48–49]. A potential issue while working with the LHS can be the presence of undesired correlations among the random variables generated during the sampling process, especially with a small number of simulations [50]. Considering that herein some variables are perfectly correlated, while the others are completely uncorrelated, a post-processing is established. In fact, the correlation matrix is checked at the end of the simulation process to ensure that no unexpected correlation is present among the not-correlated variables.

In this study, the structural modelling uncertainties considered are related to two main categories, that are: i) the mechanical material properties and ii) the geometrical properties. It is to note that this work aims to characterize the vulnerability of the buildings stock for different thresholds of the *number of floors* and the *span length*. Then, 20 structural models are obtained for each of these thresholds, by simulating the selected mechanical material and geometrical uncertain parameters, as will be described in detail in Section 3.2.1. Clearly, when the *number of floors* is fixed, the *span length* is a variable and vice-versa.

A final comment regards the association of the differential settlement profiles to the structural models. In this work, 4 distribution of potential settlement profiles are used, as will be comprehensively described in Section 3.2.2. Then, the profiles are randomly imposed at the base of the considered frame columns, according to the execution of the above-mentioned 20 simulations for each distribution. Finally, the 20 structural models are completed randomly pairing up with the 20 simulations of the settlement profiles under the columns for each distribution. This procedure is well explained and detailed in literature for seismic applications with regards to the association of structural models and ground motions [7,48], and it is herein repeated for the monotonically increasing action considered in this work.

### 2.2. Structural assessment procedure

The structural assessments for the RC columns and beams are conducted according to the Italian National code [38] and its commentary [52], that are equivalent to the Eurocodes prescriptions [39,51,53] for the considered verifications. The safety checks are conducted with respect to brittle and ductile mechanisms (shear and chord rotation capacity, respectively) for the Life-Safety (*LS*) *ls*, corresponding to the Limit State of Significant Damage (*SD*) defined in Eurocode 8 [39]. This Limit State refers to seismic actions and to a certain return period of the seismic event. Nevertheless, no similar information is available for events like landslides and subsidence. Since the proposed assessment regards an ultimate Limit State condition, an "equivalent" Life Safety condition is considered to define the verifications to be done. Then, ductile and fragile (shear and joint) safety checks have been considered. However, it is to note that the capacity models for fragile safety checks are not variable when considering monotonic or cyclic actions and do not specifically depend from *LS-ls*.

The shear strength of beams and columns is calculated in accordance with [38] and [51], on the basis of a variable inclination truss model. For members with shear reinforcements (e.g., stirrups), the shear resistance, $V_{Rd}$, is assumed as the smaller value obtained through the following expressions:

$$V_{Rd,s} = A_{sw}/s \bullet z \bullet f_{ywd} \bullet \cot\theta \tag{1}$$

$$V_{Rd,max} = \alpha_{cw} \bullet b_w \bullet z \bullet \nu_1 \bullet f_{cd}/(\cot\theta + \tan\theta) \tag{2}$$

where $A_{sw}$ is the cross-sectional area of the shear reinforcement, $s$ is the spacing of the stirrups, $f_{ywd}$ is the design yield strength of the shear reinforcement, $\nu_1$ is a strength reduction factor for concrete cracked in

shear and $\alpha_{cw}$ is a coefficient taking account of the state of stress in the compression chord.

For unconfined beam-column joints without shear reinforcement, the compression and the tension resistance are adopted to assess the shear capacity, in the principal tensile stress approach. The following expressions are provided in [52] and in [53]:

$$\sigma_{jc} = N/2A_j + \sqrt{\left(N/2A_j\right)^2 + \left(V_j/A_j\right)^2} \leq 0,5 f_c(MPa) \tag{3}$$

$$\sigma_{jt} = \left| N/2A_j - \sqrt{\left(N/2A_j\right)^2 + \left(V_j/A_j\right)^2} \right| \leq 0,3\sqrt{f_c}(MPa) \tag{4}$$

The expressions (3) and (4) are respectively related to compression and tension resistance. $N$ represents the axial action in the upper column, $A_j$ represents the resistant cross section of the joint, and $V_j$ is the total joint shear.

For ductile capacity of RC beams and columns, according to [52] and [39], the total chord rotation capacity at ultimate, $\theta_u$, is evaluated through the following expression:

$$\theta_u = \frac{1}{\gamma_{el}}\left[0,016{\cdot}0,3^{\nu}{\cdot}\left(\frac{\max(0,01;\omega')}{\max(0,01;\omega)}{\cdot}f_c\right)^{0,225}{\cdot}\left(\frac{L_v}{h}\right)^{0,35}{\cdot}25^{\left(\alpha{\cdot}\rho_{sx}\frac{f_{yw}}{f_c}\right)}{\cdot}\left(1,25^{100{\cdot}\rho_d}\right)\right] \tag{5}$$

In Eq. (5), $h$ is the depth of the cross-section; $\nu$ is the axial effort acting on the compressed part of the RC section (dimensionless); $\omega$ and $\omega$' are respectively the mechanical reinforcement ratio of the tension and compression longitudinal reinforcement; $f_c$ and $f_{yw}$ are respectively the concrete compressive strength and the stirrup yielding strength, both expressed in MPa; $L_v$ is the ratio between moment and shear at the end section; $\rho_{sx}$ is the ratio of transverse steel parallel to the direction of loading; $\rho_d$ is the steel ratio of diagonal reinforcements; $\alpha$ is a confinement efficiency factor. For primary seismic elements, the $\theta_u$ is reduced by two more factors, that are the safety coefficient $\gamma_{el}$ equal to 1,50 and the factor assumed for the considered *LS-ls*, equal to 0,75. The code formulation (5) for $\theta_u$ has been calibrated for cyclic load conditions. It is worth noting that in this study the settlements imposed on the structures are not cyclical, but monotonically increasing. Nevertheless, being the only existing code formulation, the (5) is also used as a conservative formula. By the way, the ductile verifications will not be the conditioning ones for the structural failure at the considered *ls*, as will be seen in Section 3.4 and Section 3.5.

### 2.3. Fragility assessment

The fragility assessment methodology starts from the identification of the structural response parameter. According to [40] and [54], during the incremental analysis in which the settlements are scaled up, for each *maximum differential settlement* along the profile ($\delta\rho_{max}$, [12]), the corresponding critical demand to capacity ratio for the *LS-ls* ($DCR_{LS}$) is adopted as the structural response parameter. The $DCR_{LS}$ is defined as the ratio between the demand (in terms of forces or rotations) induced by the differential settlements in the structural elements, and the capacity of the same elements, according to the *LS-ls*. The ratio is evaluated for all the RC elements, and the critical $DCR_{LS}$ of the structure is the maximum $DCR_{LS}$ among all the ratios. It can refer to the failure mechanisms described in Section 2.2, that are shear, joint and ductile failures and it will be related to the mechanism bringing the structure closest to the onset of the *LS-ls*. The analysis is interested in finding the moment when the first failure in a structural element is reached, condition occurring when $DCR_{LS}$ is equal to 1. Then, with respect to the incremental analysis in terms of $\delta\rho_{max}$, the structural fragility can be expressed as the cumulative distribution function for the $\delta\rho_{max}$ values that mark the *LS-ls* threshold $DCR_{LS} = 1$ (see [40,54]). Assuming that the critical $\delta\rho_{max}$ values at the onset of the *LS-ls*, denoted as ${\delta\rho_{max}}^{DCR=1}$, are lognormally distributed, the structural fragility based on the proposed incremental procedure can be calculated as:

$$P(DCR_{LS} \geq 1 | \delta\rho_{max} = x) = P\left({\delta\rho_{max}}^{DCR=1} \leq x\right) = \Phi\left(\frac{lnx - ln\eta_{\delta\rho_{max}|DCR=1}}{\beta_{\delta\rho_{max}|DCR=1}}\right) \tag{6}$$

where $\eta_{\delta\rho_{max}|DCR=1}$ and $\beta_{\delta\rho_{max}|DCR=1}\beta_{S_a}{}^{DCR=1}$ are the median and logarithmic standard deviation (dispersion) of ${\delta\rho_{max}}^{DCR=1}$ at the onset of the *LS*. Needless to say that the fragility model parameters are $\eta_{\delta\rho_{max}|DCR=1}$ and $\beta_{\delta\rho_{max}|DCR=1}$. In particular, the intersection of incremental curves (defined by increasing values of the $\delta\rho_{max}$) with the vertical line at $DCR_{LS} = 1$ defines the distribution of ${\delta\rho_{max}}^{DCR=1}$. A lognormal distribution is fitted to these values data and the median and logarithmic standard deviation are derived.

Finally, it is to note the fragility curves that will be illustrated in Sections 3.4 and 3.5 are expressed not only in terms of $\delta\rho_{max}$, but also in terms of *maximum deflection ratio*, $\gamma$, defined as proposed in Burland and Wroth [12] and described in detail in Section 3.2.2. In this second case, the fragility model parameters are $\eta_{\gamma|DCR=1}$ and $\beta_{\gamma|DCR=1}$.

## 3. Numerical application

### 3.1. Case-study structures population and modelling strategies description

The proposed methodology has been applied to a set of RC buildings having a parallel plane frames structural setting. This structural setting is typical of buildings designed only for gravitational loads (referred to buildings designed before 1974 [55], in Italy), widely spread in all the Mediterranean area. The population of the frame structures has been obtained through a simulation process, by fixing some geometrical and mechanical uncertain parameters. In particular, by separately fixing the *number of floors* (*NF*) and the *span length* (*SL*) to predefined values (*NF* = 2–5-8 and *SL* = 3,50–4,75–6,00 m), 20 structural models have been obtained for each of these values, by simulating the other selected geometrical and mechanical material properties, as described in Section 3.2.1. Clearly, when the *number of floors* is fixed, the *span length* is a variable and vice-versa. This choice also derives from the desire to observe which of the two parameters influences more the structural response when ground differential settlements occur. Then, the external structural frames of the introduced buildings have been modelled, and the differential settlement profiles have been applied at the base of each column of them, following the procedure that will be illustrated in Section 3.2.2.

Each structural frame presents 4 bays, with a variable *span length* (varying from one structure to another, but the same for the 4 bays in each structural frame), and a fixed floor height equal to 3,00 m. Consequently, the total length of the simulated structural frames varies between 14,00 m and 24,00 m, as well as the height, ranging between 3,00 m and 24,00 m. The infills are supposed to be constituted by double-leaf horizontal hollow clay bricks walls with a supposed thickness of 80 + 120 mm (refer to [56]), typical of Italian and Mediterranean RC buildings stock. A variable percentage of openings (*OP*) in the infills has been considered.

The RC structural elements – beams and columns – of each considered plane external infilled structural frame, have been dimensioned through a simulated design process, according to the Italian R.D.L. [57]. It is worth to specify that, in order to estimate the cross section height ($h$) for the RC elements, the first step of the simulated design is it to fix the base value ($b$) of the element cross section. In this study, the bases of both columns and beams cross sections have been set at 0,30 m for $NF \leq 2$, 0,35 m for $3 \leq NF \leq 5$ and 0,40 m for $NF \geq 6$. Then, the values of $h$ have been estimated through the simulated design. Opportune reductions of the elements cross sections have been done for the upper floors to consider the load reduction. The variation of the geometry (*NF*,

**Table 1**
Cross sections dimensions (base $b$ and height $h$), and longitudinal and transversal reinforcement ($A_l$ and $A_t$, respectively) for beams and columns of the first floor with smaller (Min) and bigger (Max) area, among all the simulated structural frames, for fixed *SL*.

| | ***SL* = 3,50 m** | | | | ***SL* = 4,75 m** | | | | ***SL* = 6,00 m** | | | |
|---|---|---|---|---|---|---|---|---|---|---|---|---|
| | **Columns** | | **Beams** | | **Columns** | | **Beams** | | **Columns** | | **Beams** | |
| | **Min** | **Max** | **Min** | **Max** | **Min** | **Max** | **Min** | **Max** | **Min** | **Max** | **Min** | **Max** |
| ***b* [cm]** | 30 | 40 | 35 | 40 | 30 | 40 | 35 | 40 | 30 | 40 | 35 | 40 |
| ***h* [cm]** | 35 | 50 | 30 | 30 | 45 | 70 | 50 | 55 | 45 | 110 | 65 | 85 |
| $A_l$ | 4Φ14 | | 5Φ14 | | 8Φ14 | | 8Φ14 | | 12Φ14 | | 11Φ14 | |
| $A_t$ | Φ6/15'' | | Φ6/10'' | | Φ6/15'' | | Φ6/5'' | | Φ6/15'' | | Φ6/5'' | |

**Table 2**
Cross sections dimensions (base $b$ and height $h$), and longitudinal and transversal reinforcement ($A_l$ and $A_t$, respectively) for beams and columns of the first floor with smaller (Min) and bigger (Max) area, among all the simulated structural frames, for fixed *NF*.

| | ***NF* = 2** | | | | ***NF* = 5** | | | | ***NF* = 8** | | | |
|---|---|---|---|---|---|---|---|---|---|---|---|---|
| | **Columns** | | **Beams** | | **Columns** | | **Beams** | | **Columns** | | **Beams** | |
| | **Min** | **Max** | **Min** | **Max** | **Min** | **Max** | **Min** | **Max** | **Min** | **Max** | **Min** | **Max** |
| ***b* [cm]** | 30 | 30 | 30 | 30 | 35 | 35 | 35 | 35 | 40 | 40 | 40 | 40 |
| ***h* [cm]** | 30 | 45 | 40 | 85 | 40 | 75 | 35 | 65 | 50 | 110 | 30 | 60 |
| $A_l$ | 4Φ14 | | 8Φ14 | | 10Φ14 | | 8Φ14 | | 16Φ14 | | 9Φ14 | |
| $A_t$ | Φ6/15'' | | Φ6/5'' | | Φ6/15'' | | Φ6/5'' | | Φ6/15'' | | Φ6/5'' | |

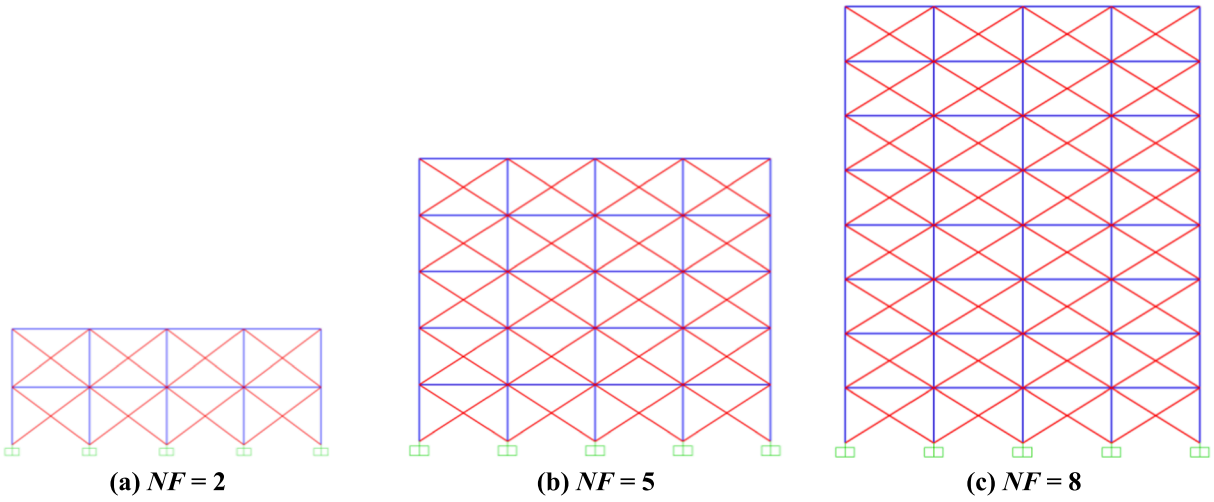


**Fig. 2.** 2D infilled structural frame models for different *NF*: 2 (a), 5 (b) and 8 (c).

**Table 3**
Summary of the considered uncertainty in the structural parameters.

| Parameter | | Distribution | | | Reference |
|---|---|---|---|---|---|
| | | Type | $p_1$ | $p_2$ | |
| Mechanical materials properties | $f_c$ [MPa] | lognormal | 29,33 | 0,31 | Verderame et al. (2001) |
| | $f_y$ [MPa] | lognormal | 356,80 | 0,19 | STIL software ReLUIS (2019) |
| | $E$ [MPa] | lognormal | 1255,00 | 0,22 | Ricci et al. (2018) |
| | $G$ [MPa] | lognormal | 315,00 | 0,11 | Ricci et al. (2018) |
| | $t_o$ [MPa] | lognormal | 0,23 | 0,05 | Ricci et al. (2018) |
| Geometrical properties | *OP* [-] | uniform | 0,20 | 0,50 | Al Chaar (2002) Gaetani d'A. et al. (2019) |
| | *SL* [m] | uniform | 3,50 | 6,00 | Gaetani d'A. et al. (2019) |
| | *NF* [-] | uniform | 2 | 8 | Borzi et al. (2008) |

*SL* and *OP*) affects the load analysis. In fact, for each simulated frame model, a corresponding load analysis is needed. Therefore, the cross sections of all RC elements are different for each model. The dimensions of the first-floor members cross sections are summarized in Table.1 and Table.2. As expected, for the first-floor columns, the cross section area increases with the number of floors. For the beams, instead, the cross section area increases with the span length. The summary of the longitudinal and transversal reinforcement ($A_l$ and $A_t$, respectively), designed through the simulated design process, is also reported in Table.1 and Table.2. For the beams, $A_l$ is referred to the longitudinal tense bars, while the longitudinal compressed ones, not indicated in the Tables, are 2Φ14.

Based on the lognormal distributions obtained using literature indications, the mechanical parameters assumed for steel, concrete and hollow clay bricks have been defined through the simulation process presented in Section 3.2.1. Smooth bars with a variable yield strength $f_y$, and an elastic modulus $E_s$ of 210000 MPa have been considered. Coherently to the variable concrete strength, $f_c$, the concrete elastic modulus, $E_c$, has been obtained based on the expression $E_c = 22000 \cdot$

**Table 4**
Correlation matrix between the uncertain parameters.

| | $f_c$ | $f_y$ | $E$ | $G$ | $t_o$ | $OP$ | $SL$ | $NF$ |
|---|---|---|---|---|---|---|---|---|
| $f_c$ | **1,00** | −0,01 | −0,24 | −0,23 | −0,21 | 0,08 | 0,20 | 0,00001 |
| $f_y$ | −0,01 | **1,00** | −0,23 | −0,23 | −0,24 | 0,06 | −0,20 | 0,16 |
| $E$ | −0,24 | −0,23 | **1,00** | 1,00 | 0,98 | 0,01 | −0,12 | 0,18 |
| $G$ | −0,23 | −0,23 | 1,00 | **1,00** | 0,99 | 0,04 | −0,13 | 0,20 |
| $t_o$ | −0,21 | −0,24 | 0,98 | 0,99 | **1,00** | 0,12 | −0,15 | −0,22 |
| $OP$ | 0,08 | 0,06 | 0,01 | 0,04 | 0,12 | **1,00** | −0,10 | −0,14 |
| $SL$ | 0,20 | −0,20 | −0,12 | −0,13 | −0,15 | −0,10 | **1,00** | −0,08 |
| $NF$ | 0,00001 | 0,16 | 0,18 | 0,20 | −0,22 | −0,14 | −0,08 | **1,00** |

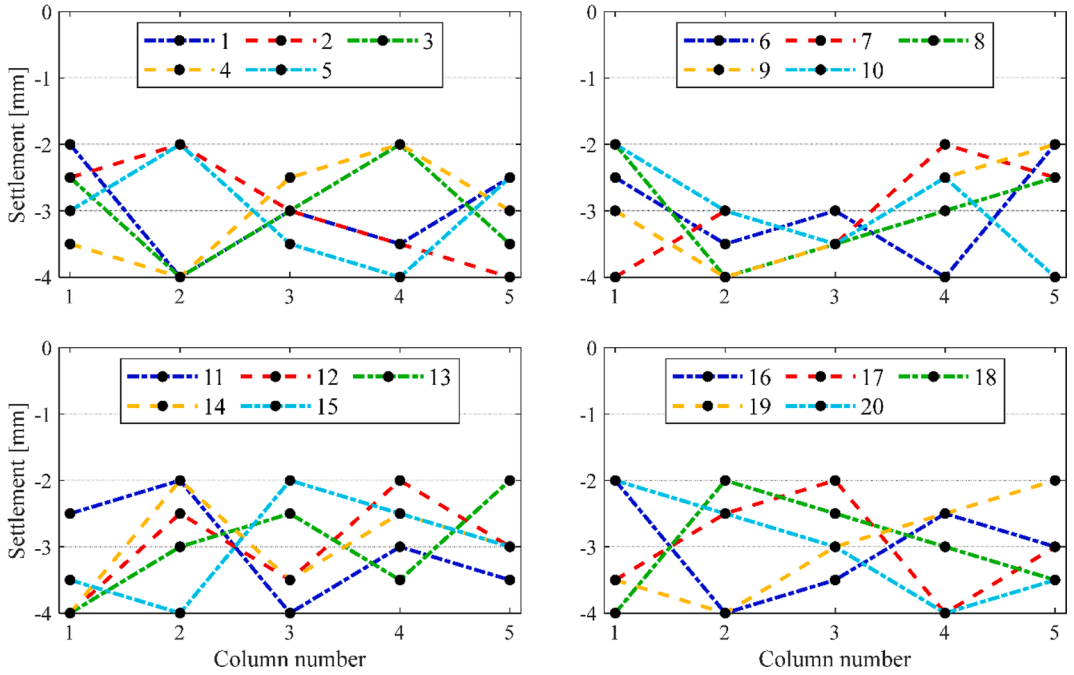


**Fig. 3.** Shapes of the 20 first base simulated settlement profiles, divided in groups of 5.

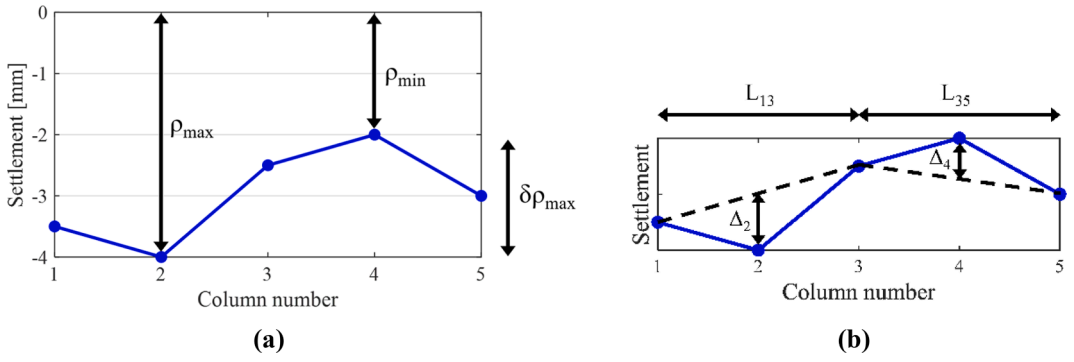


**Fig. 4.** Parameters used to quantify the magnitude of displacement inducing failure in a RC element: (a) *maximum differential settlement* $\delta\rho_{max}$; (b) identification of relative deflection Δ and distance between the reference points $L$ for sagging and hogging stretches of the profile, to evaluate the *deflection ratio*.

$(f_c/10)^{0.3}$ (with $f_c$ in MPa), provided in [38]. The mechanical properties of the hollow clay bricks are expressed in terms of elastic modulus $E$ (parallel to holes), shear modulus $G$, and tensile strength $t_o$.

The structural models for plane frames have been created using the SAP2000 software (v. 21.0.2). Beams and columns have been modeled as 2-D elements, as well as the infills, that have been reproduced as a couple of diagonal struts. Diaphragms at each level simulate the in-plane slab stiffness, as requested by the design code [57]. The presence of foundations is taken into account by fixing the bases of the first floor columns, constraining displacements in the horizontal and vertical directions. The differential settlements are applied as displacement at support at the bases of the first-floor columns. The inelastic response of the infilled structural frames used in this study has been simulated by using nonlinear structural models from literature. Columns and beams have been modeled as elastic frame elements with lumped plasticity. The inelastic response of RC members has been reproduced by introducing one inelastic rotational flexural hinge at the two ends of each frame element, according to a modeling approach specifically

```
%%  create API helper object
a  = NET.addAssembly(APIDLLPath);
helper  = SAP2000v1.Helper;
helper  = NET.explicitCast(helper,'SAP2000v1.cHelper');

if  AttachToInstance
    %%  attach to a running instance of Sap2000
    SapObject  = helper.GetObject('CSI.SAP2000.API.SapObject');
    SapObject  = NET.explicitCast(SapObject,'SAP2000v1.cOAPI');
else
    if  SpecifyPath
        %%  create an instance of the SapObject from the specified path
        SapObject  = helper.CreateObject(ProgramPath);
    else
        %%  create an instance of the SapObject from the latest installed
SAP2000
        SapObject  = helper.CreateObjectProgID('CSI.SAP2000.API.SapObject');
    end
    SapObject  = NET.explicitCast(SapObject,'SAP2000v1.cOAPI');
    %%  start Sap2000 application
    SapObject.ApplicationStart;
end
helper  = 0;
```

**Fig. 5.** Extract of the *Open Application Programming Interface* functions used in the implemented code to start SAP2000 application.

elaborated for RC members with plain bars [32]. The shear and joint failures have been considered in post-processing. This procedure is considered reliable, since the aim of this work is only the identification of the first failure at *LS-ls*. Then, with respect to the goal of the fragility curves derivation, the incremental analysis is meaningful up to the first element failure. The infills have been modelled by in-plane equivalent diagonal struts, carrying loads only in compression. Geometries of the equivalent struts have been defined according to [58], taking into account the percentage of openings through a reductive factor for the equivalent strut width. The lateral response, following the equivalent single strut model proposed by [33], has been assigned as axial hinges at the middle cross section of each diagonal frame element.

As an example, the 2D infilled structural frame models for *number of floors* equal to 2–5-8 are depicted in Fig. 2 a, b and c respectively. Each of this configuration is then specified in 20 different structural models based on the different properties coming from the outcomes of the simulation process.

### 3.2. Characterization of the uncertainties

The following Sections regard the uncertainties characterization, that can be split in two main parts. The first one (Section 3.2.1) is related to the uncertainty in the structural parameters necessary to develop the different structural models. The second one (Section 3.2.2), instead, is relative to the uncertainty in the representation of the differential settlement profiles.

#### 3.2.1. Uncertainty in the structural parameters

The parameters related to the mechanical materials properties and the geometrical properties, and their uncertainties, are summarized in Table. 3, where the columns $p_1$ and $p_2$ represent the median and the coefficient of variation (COV) in case of lognormally distributed parameters, or the minimum and the maximum values in case of uniformly distributed variables. All the mechanical materials properties have been considered to be lognormally distributed. The concrete compressive and the steel yielding strengths are denoted respectively as $f_c$ and $f_y$. Their median values and COV have been derived from available results in literature ([59] for concrete and [60] for the steel), selecting a window for the year of construction coherently with the assumptions about the set of considered RC buildings. With regards to the infills, the median and the COV for the 3 uncertain properties of construction material – the elastic modulus $E$, the shear modulus $G$ and the tensile strength $t_o$ – have been selected coherently with [61]. All the geometrical properties – *NF*, *SL* and *OP* – have been considered to be uniformly distributed. According to Bal et al. [62], the most frequent value for the opening percentage within the RC building stock in Turkey is 20%. However, as also mentioned in G. d'Aragona et al. [63], there might be cases where the *OP* is much larger. According to Al-Chaar et al. [58], if the area of the openings is greater than or equal to 60% of the area of the infill panel, then the effect of the infill should be neglected. In this work, a uniform distribution between 20% and 50% (with a simulation step of 1%) has been considered. The uniform distribution of the *span length* varies between a minimum value of 3,50 m and a maximum value of 6,00 m (with a simulation step of 0,01 m), as proposed in G. d'Aragona et al. [63]. It is to note that also in the case in which the total plan dimension of the frame is maximized (24,00 m), this length does not exceed the limit for the thermal expansion joint prescribed in the design code [57]. Finally, a variable *number of floors*, ranging from 2 to 8 (with a simulation step of 1), is identified, as proposed in Borzi et al. [64] and in good agreement with Hak et al. [65] and G. d'Aragona et al. [63].

The correlation matrix between all pairs of 8 uncertain parameters is shown in Table. 4. The three uncertain mechanical properties of construction material for the infills – the elastic modulus $E$, the shear modulus $G$ and the tensile strength $t_o$ – depend each other and a full correlation structure has been considered. It is known that $E$ and $G$ are correlated by the general Hook formulation ($G = \frac{E}{2(1+\nu)}$). Moreover, the tensile strength is the value of the maximum stress that a material can handle. This is the limit between plasticity zone and rupture zone. Then, it is meaningful to consider a full correlation among the three values (e.g., if one takes the lowest bound of the distribution for $E$, it is logical to take the lowest bound of the distribution also for $G$). The other uncertain parameters are instead independent. Then, considering that the variables in this work are perfectly correlated ($E$, $G$ and $t_o$, correlation value equal to 1) or completely uncorrelated (all the other variables), a post-processing has been established. In fact, to solve this problem, the correlation matrix has been checked at the end of the simulation process to ensure that no unexpected correlation was present among the not-correlated variables. In the case study, spurious correlations in the

**Table 5**
Prevailing failure mechanisms at *LS-ls*, for fixed *NF*.

| ***NF*** **\Direction** | **H** | **V** | **P-H** | **P-V** |
|---|---|---|---|---|
| $NF = 2$ | **Shear Joint (tension)** In about the 70–75% of the cases, the first failure regards an external joint of the 2nd floor. | | | The first failure regards in similar percentage a joint of the 1st and of the 2nd floor, with similar percentage between internal and external joints. |
| $NF = 5$ | **Shear Column /Shear Joint (tension)** In the 75% of cases, the first failure regards a 1st floor column. In the remaining cases, the first failure regards mainly an external joint of the last two floors. | **Shear Joint (tension)** The first failure always regards an external joint: of the last two floors (both 40%), or of the 1st floor (20%). | **Shear Column /Shear Joint (tension)** The first failure regards, in similar percentage, a 1st floor column or a joint, predominantly external in the last two floors. | **Shear Joint (tension) /Shear Column** The first failure regards an external joint of the 4th floor (45%) or of the 5th floor (30%). Only for one case, the first failure is in a 1st floor column. |
| $NF = 8$ | **Shear Column** The first failure regards always a 1st floor column. | **Shear Joint (tension)** In all the cases, the first failure regards a joint: one of the 1st floor (30%), one of the 3rd or 5th floor (10%) or one of the last two floors (30% and 20%, respectively). | **Shear Column /Shear Joint (tension)** In all the cases except one, the first failure regards a 1st floor column. Only for one case, the first failure regards an external joint of the last floor. | **Shear Joint (tension) /Shear Column** The first failure regards a joint (55%), predominantly of the 1st or last two floors (internal or external in similar percentage), or a 1st floor column (45%). |

order of maximum 0,24 (for 20 simulations) are found in case of zeros target correlations and can be considerable negligible with respect to the main goal of the paper.

#### 3.2.2. Uncertainty in the representation of the differential settlements

In this work, the simulated differential settlements have been imposed on the structural frames in order to observe their effects in terms of failures in the structural elements. These settlements can have origin from various kinds of actions, but the goal of the work it is not to identify their causes, but to analyze their effects on the RC buildings stock.

The defined simulated settlement profiles are characterized by various shapes and directions. With regards to the shape, 20 simulations of a base profile have been established, constituted by 5 significant points corresponding to the 5 columns of the structural frame. These 20 simulations are then associated to the 20 structural models, as explained in Section 2.1. Indicating each of the columns displacement as $\rho_i$, with $i$ ranging from 1 to 5, the minimum ($\rho_{min}$) and the maximum ($\rho_{max}$) displacements of the first base profile are imposed at 2 mm and 4 mm, respectively, for a differential settlement $\Delta\rho$ amounting to 2 mm. The remaining 3 settlements have values equally distributed between the minimum and the maximum, with an interval of 0,5 mm from each other. The 20 base profiles, in number equal to the number of simulations (as described in Section 2.2), are illustrated in Fig. 3. Among the simulated settlement profiles, segments in sagging (concavity facing upwards) and segments in hogging (concavity facing down) can be observed, including the purely U-shaped profiles typical of the literature studies. In the incremental analysis, a number of scale factors (*SF*s) have been applied to the first settlement profile of each simulation, increasing of 1 unit the multiplying factor at each increment, up to that one leading to the first structural failure, according to Section 2.2. In each scaled profile, the maximum and the minimum settlements are always in a ratio 2:1. In few cases, the profile with *SF* equal to 1, namely first base profile, was the one inducing the first structural failure. For this reason, other three preceding steps have been considered, with *SF*s equal to 0,05, 0,10 and 0,50 respectively.

The foundations settlements could have different directions, depending on the phenomenon from which they originated. To explore a range of possibilities (without going into the details of the causes, as already mentioned) the above described base profiles, gradually scaled, have been applied along 4 directions: i) horizontal (H), ii) vertical (V), iii) pseudo-horizontal (P-H) and iv) pseudo-vertical (P-V). In particular, in the P-H case, the base settlements are mainly horizontal, but are assumed to be inclined with respect to the horizontal direction such that the horizontal component is equal to 2/3 $\rho_i$ and the vertical component is equal to 1/3 $\rho_i$. Similarly, in the P-V case, the base settlements are mainly vertical, but are assumed to be inclined with respect to the vertical direction in such a manner that the horizontal component is equal to 1/3 $\rho_i$ and the vertical component is equal to 2/3 $\rho_i$. The profiles have been randomly imposed at the base of the considered frame columns as displacement at supports, based on the executed simulation (Section 2.1). The interaction between the soil and the structure has not been considered, hence the differential settlements are transmitted directly to the foundations. This is a widespread assumption for the assessment of the response of a flexible structure affected by ground movements [66]. The possible combinations between entity and direction of settlements are infinite; however, the cases presented in this work constitute an exhaustive sample of possibilities, thanks to the simulation procedure and the consideration of the possible different directions. Clearly, the action of the illustrated settlements imposed under the considered structural frame has been applied starting from the deformed condition derived from the non-linear gravity loads existence.

In Fig. 4, a, the $\rho_{min}$, $\rho_{max}$ and $\delta\rho_{max}$ are indicated for a generic settlement profile. As well, in Fig. 4, b, the dimensions needed to estimate the *deflection ratio* $\gamma = \Delta/L$ are shown for the two parts of the same settlement profile. In general, $\Delta$ is the relative deflection of sagging and hogging, namely the maximum displacement relative to the straight line connecting two reference points, and $L$ is the distance between them [12] (in Fig. 4, b, $\gamma_{13} = \Delta_2/L_{13}$ and $\gamma_{35} = \Delta_4/L_{35}$).

### 3.3. MATLAB-SAP 2000 integrated use

Fixing one by one the *number of floors* and the *span length*, the loads acting on the specific structural frame change. According to the simulation method explained in Section 2.1, for each structural frame having a fixed *number of floors* or a fixed *span length* (the 6 starting fixed values), 20 structural models have been obtained. In summary, the number of adopted models is 6 (number of the starting fixed values) times 20 (number of simulations), namely 120 models, each different from the other for geometry. As described in Section 3.1.2, the 4 different displacement profiles characterized by different shapes and directions have been randomly applied at the base of each column, based on the

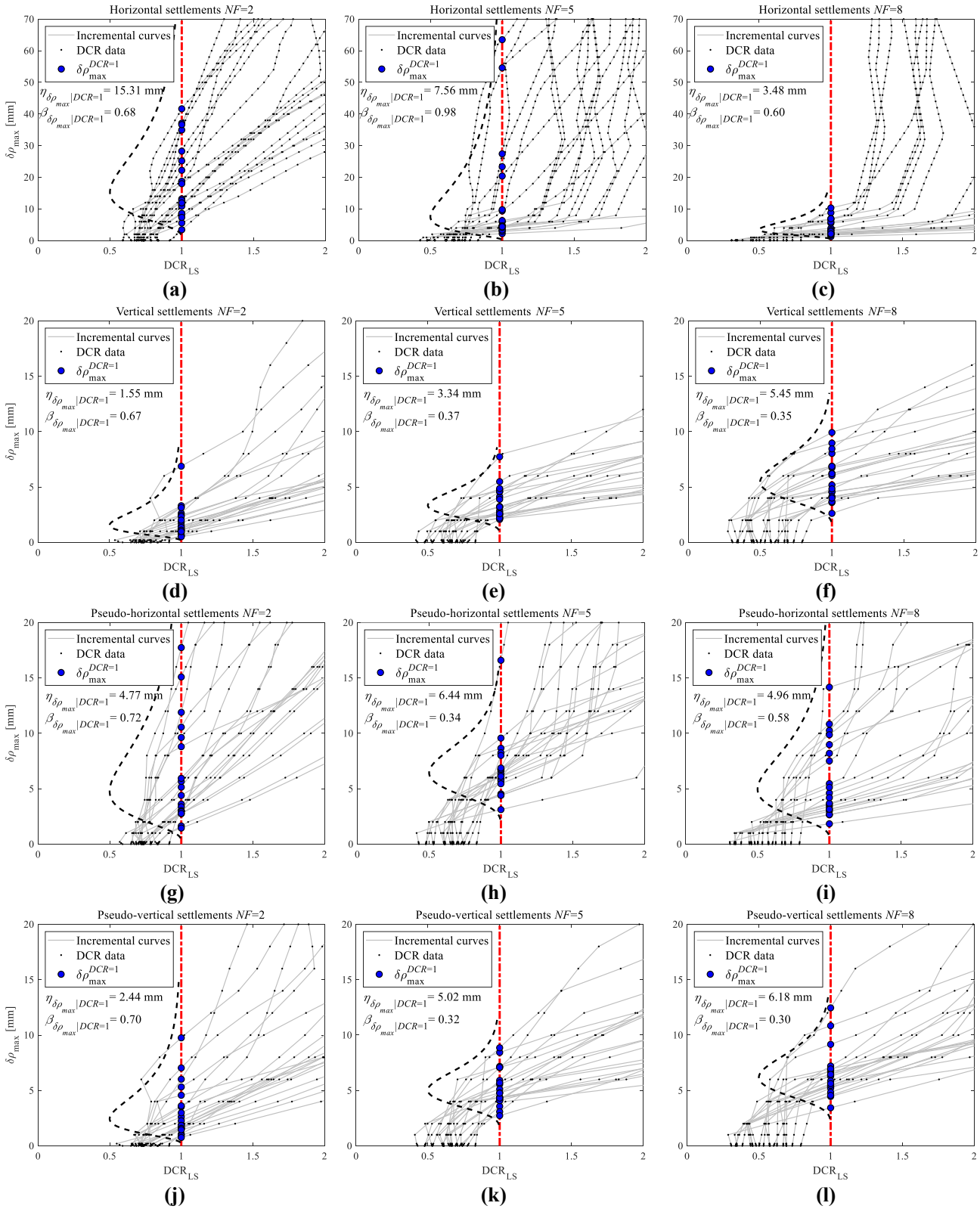


**Fig. 6.** The incremental analysis curves and the values of the $\delta\rho_{max}{}^{DCRLS=1} = 1$ for horizontal (a,b,c), vertical (d,e,f), pseudo-horizontal (g,h,i) and pseudo-vertical (j, k,l) differential settlements, in case of fixed *NF*.

executed simulation. These displacement profiles have been incremented with a predefined step up to the point in which the first failure is attained. For operational simplicity, all the 120 models obtained by fixing one basic parameter have been replied 4 times, one time for every different displacement profile direction, for a total number of 480 models.

The large number of structural frames models to be analyzed makes the implementation of the analysis and the drafting of the structural checks very expensive. In order to reduce the computational burden, the *Open Application Programming Interface* (OAPI) by CSI [30] has been

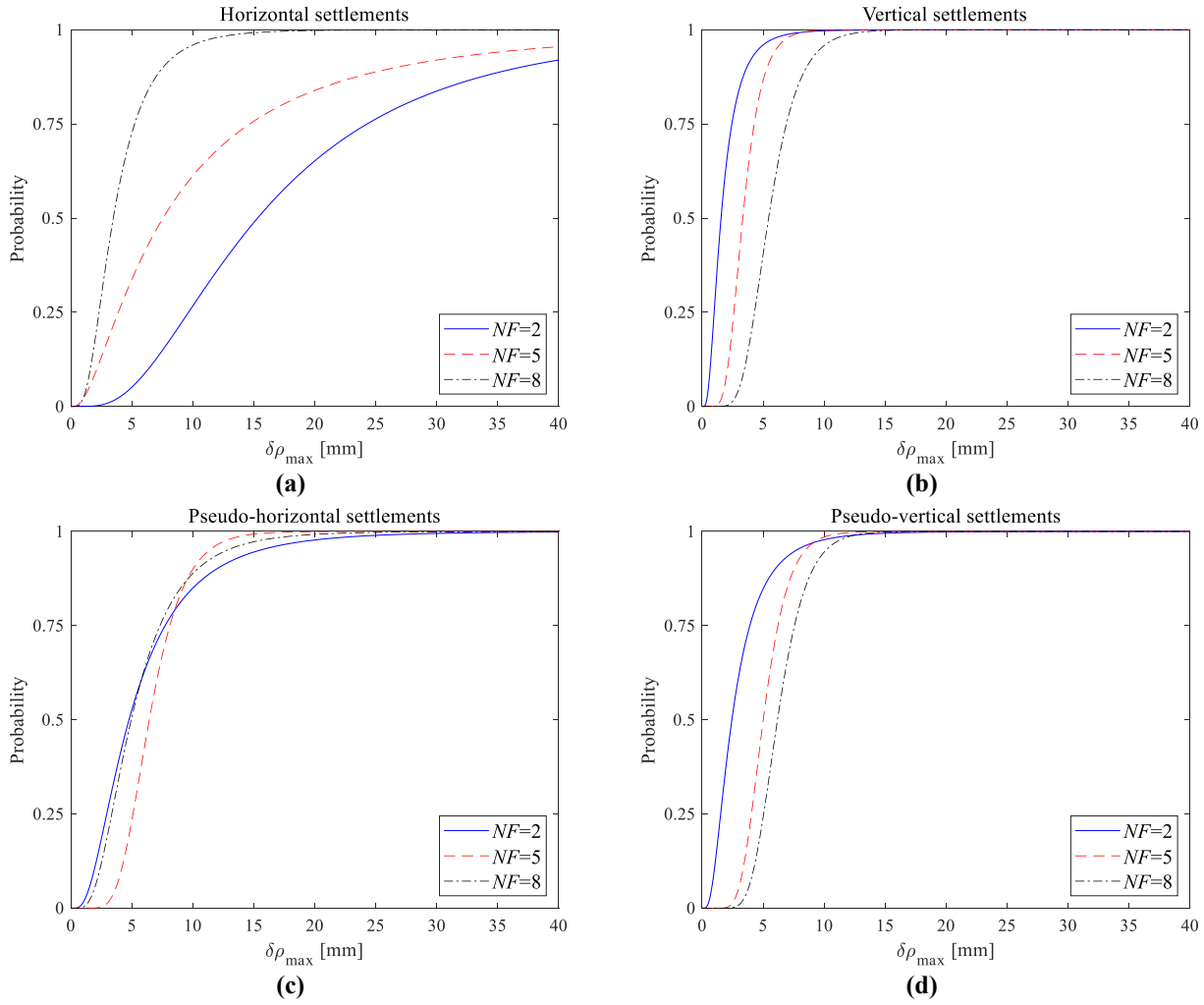


**Fig. 7.** Comparison among the fragility curves in terms of $\delta\rho_{max}$ for *LS-ls*, associated with the different fixed *NF* and under the different types of differential settlement profiles.

**Table 6**
Statistical parameters for fragility curves at LS-ls, for fixed NF, considering as structural response parameter $\delta\rho_{max}$.

| Analysis case | η [mm] | β | Analysis case | η [mm] | β | Analysis case | η [mm] | β |
|---|---|---|---|---|---|---|---|---|
| H_*NF* = 2 | 15,31 | 0,68 | H_*NF* = 5 | 7,56 | 0,98 | H_*NF* = 8 | 3,48 | 0,60 |
| V_*NF* = 2 | 1,55 | 0,67 | V_*NF* = 5 | 3,34 | 0,37 | V_*NF* = 8 | 5,45 | 0,35 |
| P-H_*NF* = 2 | 4,77 | 0,72 | P-H_*NF* = 5 | 6,44 | 0,34 | P-H_*NF* = 8 | 4,96 | 0,58 |
| P-V_*NF* = 2 | 2,44 | 0,70 | P-V_*NF* = 5 | 5,02 | 0,32 | P-V_*NF* = 8 | 6,18 | 0,30 |

implemented for use in a complementary way the structural modelling software SAP2000 and the code software MATLAB, that uses a high-performance language for technical computing based on matrixes. The MATLAB code language has been exploited to start SAP2000, build the models, and launch the analysis from an external application, though also other languages could be used to access SAP2000 OAPI functions (e.g., Visual Basic). The procedure is explained in the following with reference to one structural frame model.

The input elements for the MATLAB script where OAPI functions have been implemented are: i) the geometrical properties of beams, columns and infills, ii) the simulated parameters needed to create the model and iii) the characteristic points of the curves describing the plastic hinges non-linear behavior, related to RC elements and infills struts, described in Section 3.1. All the geometrical properties of beams, columns and infills, both the fixed properties and those obtained after implementing the simulated design, have been grouped in a *structure array*, a data type that collect related data using data containers called *fields*. As well, the simulated parameters and the defined plastic hinges needed to create the model have been imported in the code. It is worth noting that when the *number of floors* has been fixed, the *span length* has been considered as a simulated parameter, and vice-versa, when the *span length* has been fixed, the *number of floors* has been considered as a simulated parameter. The elements in ii) and iii) have been imported as matrixes in *.mat* format files. An extract of the implemented code used to start SAP2000 application is reported in Fig. 5.

The whole process implemented in MATLAB can be summarized as: 1) calculation of the building parameters (material and geometric properties of beams, columns and infills), with uncertainty; 2) writing down of the OAPI commands to create the structural model in SAP2000; 3) editing of the *.$2k* format file generated by SAP2000 to add some necessary elements of the structural model, such as the diaphragm

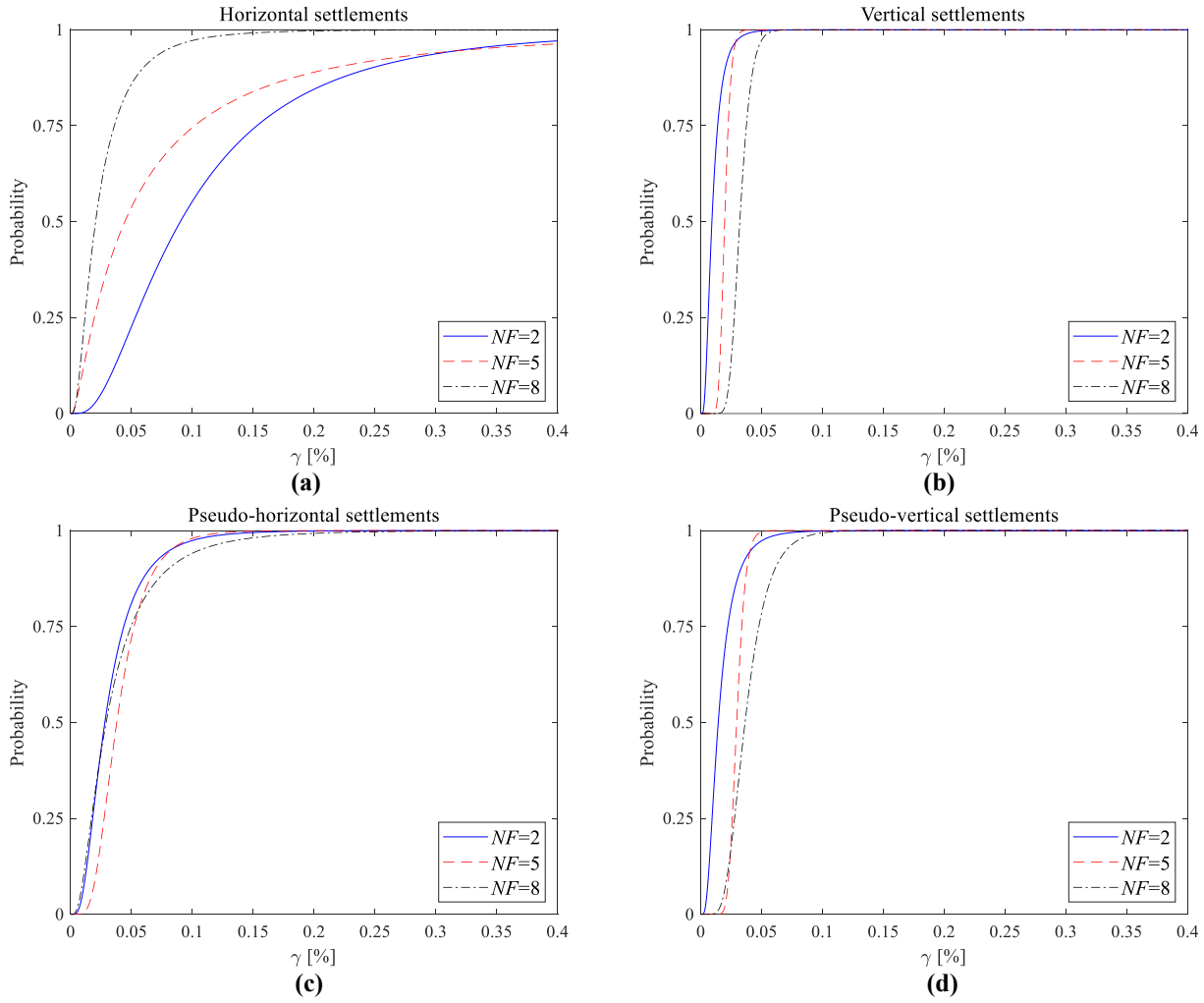


**Fig. 8.** Comparison among the fragility curves in terms of γ for *LS-ls* associated with the different fixed *NF* and under the different types of differential settlement profiles.

**Table 7**
Statistical parameters for fragility curves at *LS-ls*, for fixed NF, considering as structural response parameter $\gamma$.

| Analysis case | η [%] | β | Analysis case | η [%] | β | Analysis case | η [%] | β |
|---|---|---|---|---|---|---|---|---|
| H_*NF* = 2 | 0,09 | 0,79 | H_*NF* = 5 | 0,04 | 1,23 | H_*NF* = 8 | 0,02 | 0,83 |
| V_*NF* = 2 | 0,01 | 0,62 | V_*NF* = 5 | 0,02 | 0,20 | V_*NF* = 8 | 0,03 | 0,23 |
| P-H_*NF* = 2 | 0,03 | 0,65 | P-H_*NF* = 5 | 0,04 | 0,47 | P-H_*NF* = 8 | 0,03 | 0,79 |
| P-V_*NF* = 2 | 0,01 | 0,65 | P-V_*NF* = 5 | 0,03 | 0,20 | P-V_*NF* = 8 | 0,04 | 0,40 |

constraints at each floor, the gravitational loads, the ground settlement profiles and the plastic hinges related to beams, columns and struts; 4) opening of the complete *.$2k* format file in SAP2000 and running of the analyses of the structural model.

All what described for one single model has been repeated for the 480 models previously introduced, setting two loops in the code: the first loop on the number of simulations, varying from 1 to 20 (Section 2.1); the second loop on the number of displacement profiles to apply at the base of the columns, varying from 1 to 4 (Section 3.1.2). This has been repeated for each of the 6 fixed basic parameters values. Thanks to the implemented procedure, all the steps of the model creation and analysis have been automatized, for all the models to be created. Editing the *.$2k* files in MATLAB, as suggested, makes it very fast to create structural models in SAP2000, complete of all the features and the loads, easily allowing to run analysis without the intervention of the engineer, who in any case performs a post-clearance check of the results.

### 3.4. Fragility curves by fixing the number of floors

For each fixed *number of floors*, the results about the incremental analyses and the fragility curves are shown in this Section. The incremental analysis is performed for the suite of 20 structural models, described in Section 3.2.1, by scaling up the amplitude of the settlement profiles, presented in Section 3.2.2. The 20 couples of structural models/settlement profiles are randomly associated, as discussed in Section 2.1. Before presenting incremental analysis curves and fragility curves, the structural response at *LS-ls* for the set of fixed number of floors is shown in Table. 5, where the failure mechanisms – separated for settlements direction – have been summarized.

For each case created by fixing the value of the *number of floors*, the results are shown based on the application of horizontal (Fig. 6, a-c), vertical (Fig. 6, d-f), pseudo-horizontal (Fig. 6, g-i) and pseudo-vertical (Fig. 6, j-l) differential settlements. The incremental analysis curves are

**Table 8**
Prevailing failure mechanisms at *LS-ls*, for fixed *SL*.

| *SL* \ Direction | H | V | P-H | P-V |
|---|---|---|---|---|
| *SL* = 3,50 | **Shear Joint (tension) /Shear Column** | **Shear Joint (tension)** | **Shear Joint (tension) /Shear Column** | **Shear Joint (tension)** |
| | In the 60% of cases, the first failure regards a joint (83% external, 67% at last two floors). In the remaining 40% of cases, the first failure regards a 1st floor column. | The first failure regards an external joint in the 70% of cases and a joint of the last two floors in the 65% of cases. | In all the cases except one, the first failure regards a joint: an external joint in the 60% of cases and a joint of the last two floors in the 60% of cases. For the remaining case, the first failure regards a 1st floor column. | The first failure regards an external joint in the 70% of cases and a joint of the last two floors in the 75% of cases. |
| *SL* = 4,75 | **Shear Column /Shear Joint (tension)** | **Shear Joint (tension)** | **Shear Joint (tension) /Shear Column** | **Shear Joint (tension)** |
| | In the 60% of cases, the first failure regards a 1st floor column. In the remaining cases, the first failure regards mainly an external joint of the last two floors. | The first failure regards an external joint in the 75% of cases and a joint of the last two floors in the 70% of cases. | The first failure regards a joint (55%), predominantly of the 1st or last two floors, (external at the 64%), or a 1st floor column (45%). | The first failure regards an external joint in the 70% of cases and a joint of the last two floors in the 70% of cases. |
| *SL* = 6,00 | **Shear Column /Shear Joint (tension)** | **Shear Joint (tension)** | **Shear Column /Shear Joint (tension)** | **Shear Joint (tension) /Shear Column** |
| | In all the cases except one, the first failure regards a 1st floor column. Only for one case, the first failure regards an external joint of the 2nd floor. | The first failure regards an external joint in the 70% of cases and a joint of the last two floors in the 60% of cases. | In the 90% of cases, the first failure regards a 1st floor column. In the remaining cases, the first failure is in a joint. | The first failure regards a joint (60%), predominantly of the 1st or the last two floors (external at 58%), or a 1st floor column (40%). |

plotted in thin grey lines in Fig. 6. Each curve shows the variation in the performance variable $DCR_{LS}$ as a function of $\delta\rho_{max}$, while the settlements profile's amplitude is linearly scaled-up. The analysis is of interest up to the level in which the first failure in a RC element is reached, that occur when $DCR_{LS} = 1$. The $\delta\rho_{max}$ values on the incremental analysis curves corresponding to $DCR_{LS} = 1$ and denoted as ${\delta\rho_{max}}^{DCR_{LS}=1}$(i.e., the $\delta\rho_{max}$ levels marking the onset of the limit state) are shown as blue circles on the red dashed vertical line, the latter representing the condition $DCR_{LS} = 1$. However, in order to show a more complete picture of the $\delta\rho_{max}$–$DCR_{LS}$ response, the horizontal axes is shown up to 2. The values of ${\delta\rho_{max}}^{DCR_{LS}=1}$, together with the fitted (Lognormal) probability density function (PDF), plotted as a black dashed line, are shown in Fig. 6. As well, the median and the logarithmic standard deviation (dispersion) of ${\delta\rho_{max}}^{DCR=1}$ at the onset of *LS-ls*, respectively $\eta_{\delta\rho_{max}|DCR=1}$ and $\beta_{\delta\rho_{max}|DCR=1}$, are shown in Fig. 6.

Fig. 7 shows the resulting lognormal incremental analysis-based fragility curves, respectively for horizontal (Fig. 7, a), vertical (Fig. 7, b), pseudo-horizontal (Fig. 7, c) and pseudo-vertical (Fig. 7, d) differential settlements, correlated to the probability of exceedance of the *LS-ls* due to the first RC element failure. In each figure, the solid blue line represents the fragility curve for the structural models with fixed $NF = 2$, the dashed red line proposes the fragility curve for the structural models with fixed $NF = 5$ and the dot-dashed black line presents the fragility curve for the structural models with fixed $NF = 8$. All the curves are cut at $\delta\rho_{max}$ equal to 40 mm, to have a uniform view of the differences between the various directions of application of the differential settlement.

The vulnerability trend at *LS-ls* among the suite of buildings with *number of floors* equal to 2, 5 and 8 is opposite when the horizontal and the vertical settlements are applied. In fact, under horizontal settlements, the more the *number of floors* increases, the more the buildings stock is vulnerable. On the other side, under vertical settlements, the more the *number of floors* decreases, the more the buildings stock is vulnerable. It is to note that the vertical settlements induce a prevalent mechanism related to the failure of the beam-column joints without shear reinforcement, as shown in Table. 5. Under horizontal settlements, instead, there are two prevalent mechanisms (that are joints failures and shear crises in the columns). In particular, with the increasing of the *number of floors*, the number of governing shear crises in the columns raises up, becoming prevalent when the *number of floors* is 8. With respect to pseudo-horizontal settlements, when the *number of floors* is low, the introduced vertical component of the displacement induces joints failures for lower steps of the analysis with comparison to the case of total horizontal settlements, reducing the median capacity (see Table. 6, H_$NF = 2/5$ versus PH_$NF = 2/5$). From the other side, this effect is opposite when the *number of floors* is higher, increasing a little bit the capacity in terms of $\eta_{\delta\rho_{max}|DCR=1}$, (see Table. 6, H_$NF = 8$ versus PH_$NF = 8$). Instead, the trend of the fragility curves is confirmed between vertical and pseudo-vertical direction of application of the settlements for all the considered cases. In the latter case, there is a small amount in the capacity in terms of $\eta_{\delta\rho_{max}|DCR=1}$, more sensible when the *number of floors* is low. All the statistics of these curves in terms of median and standard deviation are reported in Table. 6 (where $\eta = \eta_{\delta\rho_{max}|DCR=1}$ *and* $\beta = \beta_{\delta\rho_{max}|DCR=1}$).

The fragility curves have been obtained also using γas structural response parameter. The resulting lognormal incremental analysis-based fragility curves, correlated to the probability of exceedance of the *LS-ls* due to the first RC element failure, are presented, respectively for horizontal (Fig. 8, a), vertical (Fig. 8, b), pseudo-horizontal (Fig. 8, c) and pseudo-vertical (Fig. 8, d) differential settlements. The legend of the figure is the same of Fig. 7.

Clearly, also considering γ as structural response parameter, the vulnerability at *LS-ls* of the suite of buildings with $NF = 2$, 5 and 8 is opposite when the horizontal and the vertical settlements are applied, with a trend of the fragility curves similar to what happens with $\delta\rho_{max}$. The same trend between horizontal/vertical and pseudo horizonal/vertical settlements directions, described for $\delta\rho_{max}$, is confirmed. Finally, the statistical parameters for fragility curves in terms of γ are proposed in Table. 7 (where $\eta = \eta_{\gamma|DCR=1}$ and $\beta = \beta_{\gamma|DCR=1}$).

### 3.5. Fragility curves by fixing the span length

For each fixed *span length*, the results about the incremental analysis and the fragility curves are shown in this Section. Also in this case, the incremental analysis is performed for the suite of 20 structural models, by scaling up the amplitude of the settlement profiles. The structural

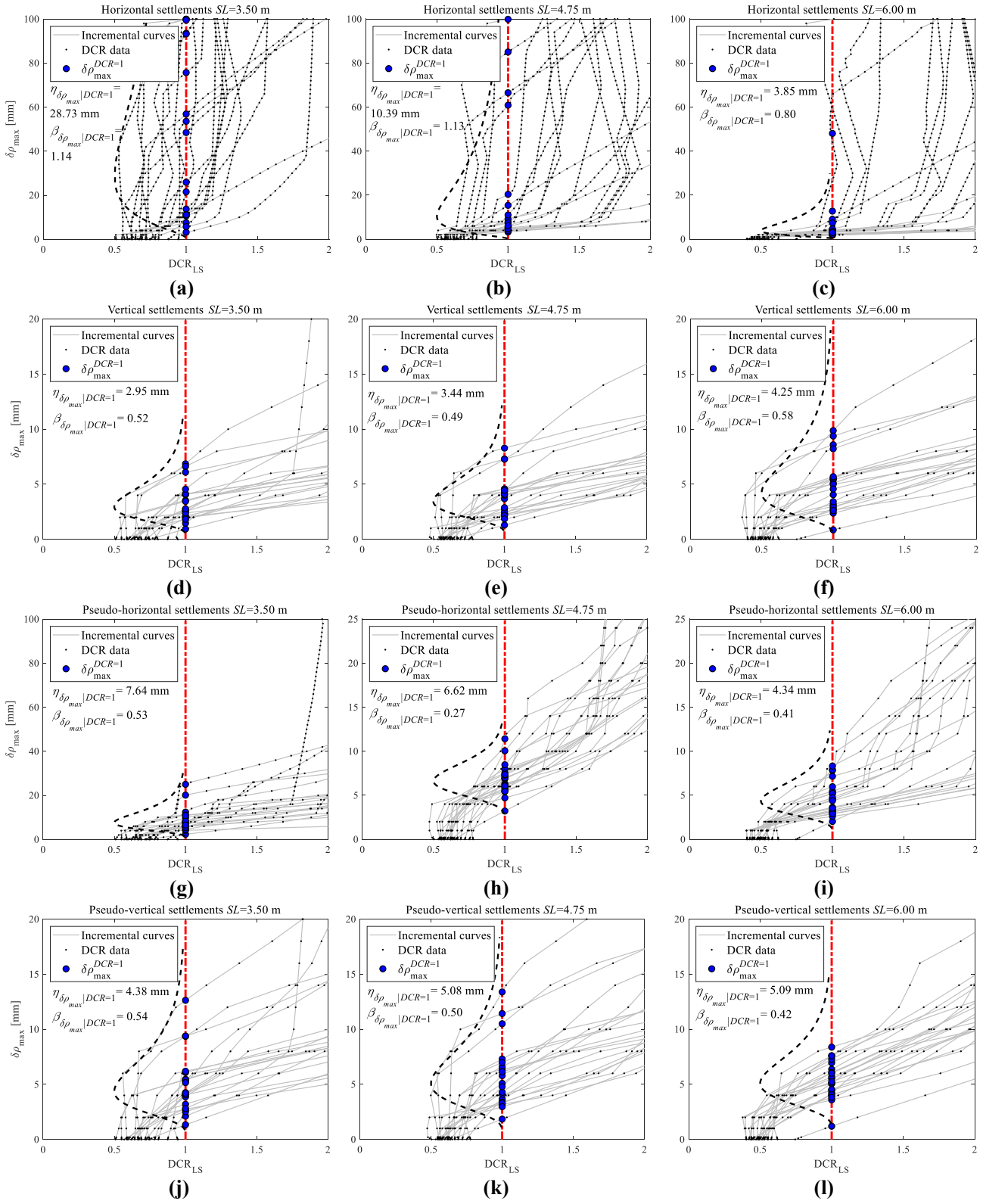


**Fig. 9.** The incremental analysis curves and the values of the $\delta\rho_{max}{}^{DCRLS=1} = 1$ for horizontal (a,b,c), vertical (d,e,f), pseudo-horizontal (g,h,i) and pseudo-vertical (j, k,l) differential settlements, in case of fixed *SL*.

response at *LS-ls* for the set of fixed span length is shown in Table. 8, where the failure mechanisms – separated for settlements direction – have been summarized.

For each fixed value of the *span length*, the results are shown based on the application of horizontal (Fig. 9, a-c), vertical (Fig. 9, d-f), pseudo-horizontal (Fig. 9, g-i) and pseudo-vertical (Fig. 9, j-l) differential settlements. The legend of the figure is the same of Fig. 6. The values of $\delta\rho_{max}{}^{DCR_{LS}=1}$, together with the fitted (Lognormal) PDF, the values of $\eta_{\delta\rho_{max}|DCR=1}$ and $\beta_{S_a{}^{DCR=1}}$ $\beta_{\delta\rho_{max}|DCR=1}$ at the onset of *LS-ls*, are also shown in Fig. 9.

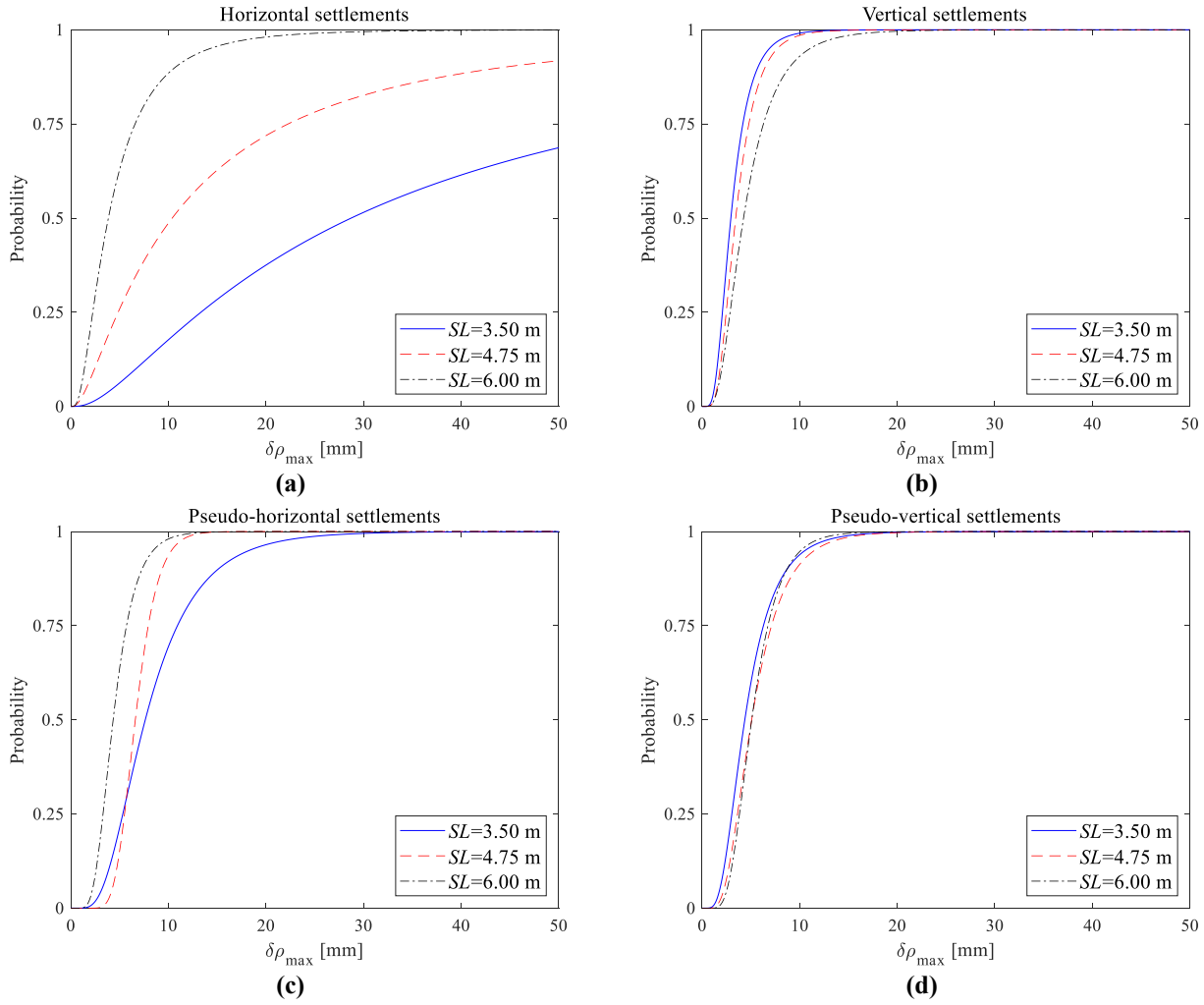


**Fig. 10.** Comparison among the fragility curves in terms of $\delta\rho_{max}$ for *LS-ls* associated with the different fixed *SL* and under the different types of settlements.

**Table 9**
Statistical parameters for fragility curves at LS-ls, for fixed SL, considering as structural response parameter $\delta\rho_{max}$.

| Analysis case | η [mm] | β | Analysis case | η [mm] | β | Analysis case | η [mm] | β |
|---|---|---|---|---|---|---|---|---|
| H_*SL* = 3,50 *m* | 28,73 | 1,14 | H_*SL* = 4,75 *m* | 10,39 | 1,13 | H_*SL* = 6,00 *m* | 3,85 | 0,80 |
| V_*SL* = 3,50 *m* | 2,95 | 0,52 | V_*SL* = 4,75 *m* | 3,44 | 0,49 | V_*SL* = 6,00 *m* | 4, 25 | 0,58 |
| P-H_*SL* = 3,50 *m* | 7,64 | 0,53 | P-H_*SL* = 4,75 *m* | 6,62 | 0,27 | P-H_*SL* = 6,00 *m* | 4,34 | 0,41 |
| P-V_*SL* = 3,50 *m* | 4,38 | 0,54 | P-V_*SL* = 4,75 *m* | 5,08 | 0,50 | P-V_*SL* = 6,00 *m* | 5,09 | 0,42 |

Fig. 10 shows the resulting lognormal incremental analysis-based fragility curves, respectively for horizontal (Fig. 10, a), vertical (Fig. 10, b), pseudo-horizontal (Fig. 10, c) and pseudo-vertical (Fig. 10, d) settlements, correlated to the probability of exceedance of the *LS-ls* due to the first RC element failure. In each figure, the solid blue line represents the fragility curve for the structural models with *SL* = 3,50 m, the dashed red line proposes the fragility curve for the structural models with *SL* = 4,75 m and the dot-dashed black line presents the fragility curve for the structural models with *SL* = 6,00 m. All the curves are cut at $\delta\rho_{max}$ equal to 50 mm, to have a uniform view of the differences between the various directions of application of the differential settlement.

The trend of vulnerability at *LS-ls* among the suite of buildings with *span length* equal to 3,50, 4,75 and 6,00 m is opposite when the horizontal and the vertical settlements are applied. In fact, under horizontal settlements, the more the *span length* increases, the more the buildings stock is vulnerable, while, under vertical settlements, the more the *span length* decreases, the more the buildings stock is vulnerable. It is to note that, under vertical settlements, there is a prevalent mechanism related to the failure of the beam-column joints without shear reinforcement, as shown in Table. 8. Under horizontal settlements, instead, there are two prevalent mechanisms (that are joints failures and shear crises in the columns). In particular, the shear crises in the columns became dominant with the increasing of the *span length*, becoming almost totally prevalent when the *span length* is 6,00 m. With respect to pseudo-horizontal settlements, when the *span length* is low, the introduced vertical component of the displacement induces prevalent joints failures, moreover for lower steps of the analysis with comparison to the case of failure for total horizontal settlements, reducing the median capacity (see Table. 9, H_*SL* = 3,50/4,75 m versus P-H_*SL* = 3,50/4,75 m). When the *span length* is higher, the median capacity of the buildings stock is comparable in all cases (see Table. 9, H_*SL* = 6,00 m, V_*SL* = 6,00 m, P-H_*SL* = 6,00 m and P-V_*SL* = 6,00 m). Instead, comparing the fragility curves for vertical and pseudo-vertical direction of application of the settlements, the trend is quite confirmed, but it is to note that for *SL* =

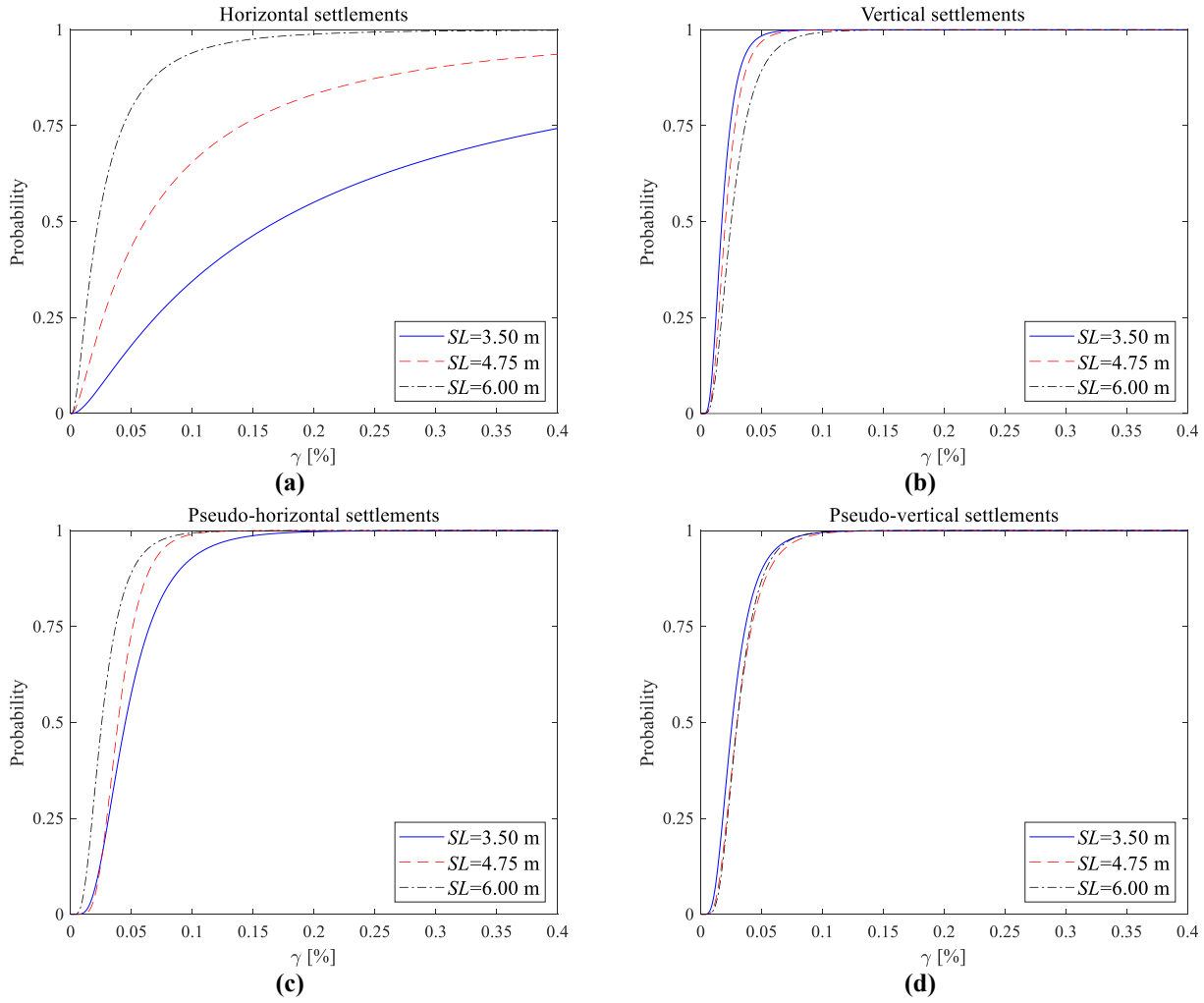


**Fig. 11.** Comparison among the fragility curves in terms of γ for *LS-ls* associated with the different fixed *SL* and under the different types of settlements.

**Table 10**
Statistical parameters for fragility curves at *LS-ls,* for fixed *SL*, considering as structural response parameter γ.

| Analysis case | η [%] | β | Analysis case | η [%] | β | Analysis case | η [%] | β |
|---|---|---|---|---|---|---|---|---|
| H_*SL* = 3,50 *m* | 0,17 | 1,32 | H_*SL* = 4,75 *m* | 0,06 | 1,23 | H_*SL* = 6,00 *m* | 0,02 | 0,96 |
| V_*SL* = 3,50 *m* | 0,02 | 0,49 | V_*SL* = 4,75 *m* | 0,02 | 0,48 | V_*SL* = 6,00 *m* | 0,02 | 0,56 |
| P-H_*SL* = 3,50 *m* | 0,04 | 0,54 | P-H_*SL* = 4,75 *m* | 0,04 | 0,40 | P-H_*SL* = 6,00 *m* | 0,03 | 0,55 |
| P-V_*SL* = 3,50 *m* | 0,03 | 0,52 | P-V_*SL* = 4,75 *m* | 0,03 | 0,50 | P-V_*SL* = 6,00 *m* | 0,03 | 0,46 |

4,75 m there is a slight improvement in the structural responses, due to the introduced horizontal components (see Table. 9, V_*SL* = 4,75 m versus P-V_*SL* = 4,75 m). All the statistics of these curves in terms of median and standard deviation are reported in Table. 9 (where $\eta = \eta_{\delta\rho_{max}|DCR=1}$ *and* $\beta = \beta_{\delta\rho_{max}|DCR=1}$).

Also in this case, the fragility curves have been additionally obtained by using γ as structural response parameter. Fig. 11 presents the resulting lognormal incremental analysis-based fragility curves, respectively for horizontal (Fig. 11, a), vertical (Fig. 11, b), pseudo-horizontal (Fig. 11, c) and pseudo-vertical settlements (Fig. 11, d). The legend of the figure is the same of Fig. 10.

Clearly, also when γ is considered as structural response parameter, the vulnerability at *LS-ls* of the suite of buildings with *SL* = 3,50, 4,75 and 6,00 m is opposite when the horizontal and the vertical settlements are applied . The trend between horizontal/vertical and pseudo horizonal/vertical settlements directions, described for $\delta\rho_{max}$, is confirmed. Finally, the statistical parameters for fragility curves considering as structural response parameter γ are proposed in Table. 10 (where $\eta = \eta_{\gamma|DCR=1}$ and $\beta = \beta_{\gamma|DCR=1}$).

The direct comparison of these results with other few indications from literature is not possible, due to the difference in methodology (analytical versus empirical methods), chosen limit/damage states, population sample (structural type, materials, geometry, etc.), type and direction of the considered settlements. In particular, one of the novelties of this work is that it provided a full compatible code assessment and then the safety checks have been done accordingly to the recommendations for Italian/European ultimate Limit State. The interesting studies that also provide a fragility assessment based on induced settlements actions used performance-based damage states. However, for vertical and pseudo-horizontal differential settlements, by comparing these statistical outcomes with the fragility curves for RC buildings proposed in [19,29], nevertheless the code based assessment is more conservative, a general agreement on the order of magnitude of the differential settlements inducing the elements failure can be found.

## 4. Conclusions

This study investigates the vulnerability of a RC infilled buildings stock with a parallel plane frames structural system with respect to imposed displacement with varying magnitudes and/or inclinations. The RC buildings population has been simulated: first the uncertain parameters related to geometrical and mechanical material properties have been identified and then the structural design of the elements by a simulated design procedure has been carried out. The computational burden deriving from the large number of FEM models to be managed has been widely reduced by integrating the structural modelling software SAP2000 and the code software MATLAB by means of the *Open Application Programming Interface* (OAPI) tool. A stock of simulated differential settlements has been randomly applied at the base of the structural RC frames. Then, time by time, a non-linear incremental analysis procedure has been implemented by scaling up the amplitude of the imposed base displacements obtained by the simulation operation. The seismic safety assessment, implemented with reference to the *LS-ls* at each step of the analysis, has allowed to find the *maximum differential settlements* (or the *deflection ratios*) tolerable in code-based terms, through the use of the critical demand to capacity ratio at the onset on the selected *ls*. These results have allowed to propose analytical fragility curves in terms of the considered geometrical features, namely the *number of floors* and the *span length*.

This work demonstrates that the geometrical features have a high impact on the frame vulnerability measures, when base differential displacements are applied. By observing the fragility curves results, the following considerations can be done. Structures with high *number of floors* or significant *span length* are more sensitive to settlements acting in purely horizontal direction. In the developed analyses, the worst condition is for *number of floors* equal to 8 or *span length* equal to 6,00 m, while the vulnerability level becomes lower with the reduction of the heigh and/or of the plan dimensions of the building. The presence of a little vertical component, even if the horizontal one is always the most significant (pseudo-horizontal settlements case) produces a reversal in the fragility trends of the two considered geometrical parameters, meaning that lower or smaller buildings are more sensitive to vertical settlements. This is confirmed by the fact that exclusively vertical settlements have the worst effect on structures with low *number of floors* or with little *span length*. In the developed analyses, the worst condition is for *number of floors* equal to 2 or *span length* equal to 3,50 m, improving with the increasing of the height and of the plan dimensions of the building. The presence of a little horizontal component (pseudo-vertical settlements case) induces a light improvement in the probability of failure for the structures in relation to the investigated differential displacements.

### *CRediT authorship contribution statement*

**Andrea Miano:** Conceptualization, Methodology, Software, Validation. **Annalisa Mele:** Conceptualization, Methodology, Software, Validation. **Andrea Prota:** Conceptualization, Methodology, Supervision.

### Declaration of Competing Interest

The authors declare that they have no known competing financial interests or personal relationships that could have appeared to influence the work reported in this paper.

### Acknowledgments

The research project reported in this paper was conducted thanks to the financial support from DCP-ReLUIS 2019-2021.

## References

[1] Liel AB, Haselton CB, Deierlein GG. Seismic collapse safety of reinforced concrete buildings. II: Comparative assessment of nonductile and ductile moment frames. J Struct Eng 2011;137(4):492–502.
[2] Fragiadakis M, Vamvatsikos D, Aschheim M. Application of nonlinear static procedures for seismic assessment of regular RC moment frame buildings. Earthquake Spectra 2013;30(2):767–94.
[3] Miano A, Sezen H, Jalayer F, Prota A. Performance-based assessment methodology for retrofit of buildings. J Struct Eng 2019;145(12):04019144. https://doi.org/10.1061/(ASCE)ST.1943-541X.0002419.
[4] Carofilis W, Perrone D, O'Reilly GJ, Monteiro R, Filiatrault A. Seismic retrofit of existing school buildings in Italy: Performance evaluation and loss estimation. Eng Struct 2020;225:111243.
[5] Vamvatsikos D, Fragiadakis M. Incremental dynamic analysis for estimating seismic performance sensitivity and uncertainty. Earthquake Eng Struct Dyn 2010; 39(2):141–63.
[6] Celarec D, Dolšek M. The impact of modelling uncertainties on the seismic performance assessment of reinforced concrete frame buildings. Eng Struct 2013; 52:340–54.
[7] Jalayer F, Ebrahimian H. Seismic reliability assessment and the nonergodicity in the modelling parameter uncertainties. Earthquake Eng Struct Dyn 2020;49(5): 434–57.
[8] Skempton AW, MacDonald DH. Allowable Settlement of Buildings, P. I. Civil Eng., 5, Part III, 727–68, 1956.
[9] Bjerrum L. Allowable Settlement of Structures. In: Proceedings of the 3rd European Conf. on Soil Mech. and Found. Engng, Wiesbaden, 2, Brighton, England, 135–7, 1963.
[10] Meyerhof GG. Discussion on paper by AW Skempton and DH MacDonald. The allowable settlement of buildings. Proc Inst Civ Eng 1956;2:774–5.
[11] Polshin DE, Tokar RA. Maximum Allowable Non-uniform Settlement of Structures. In: Proc. 4th Int. Conference Soil Mechanics and Foundation Engineering, London, Butterworths Scientific Publications, 402–5, 1957.
[12] Burland JB, Wroth CP. Settlement of buildings and associated damage. Proc Br Geotech Soc Conf Settl Struct, 611–54, 1974.
[13] Burland JB, Broms BB, De Mello VFB. Behaviour of Foundations and Structures. Proc 9th Int Conf Soil Mech Found Eng, Tokio 1977:363–400.
[14] Boscardin MD, Cording EG. Building Response to Excavation Induced Settlement. J. Geotech. Eng.-ASCE 1989;115:21.
[15] Boone SJ. Ground-Movement-Related Building Damage. J Geotechnical Eng, ASCE 1996;122(11):886–96.
[16] Poulos HG, Carter JP, Small JC. Foundations and retaining structures - Research and practice. Proc XV Int Conf Soil Mech Found Eng, Istambul 2001:2527–606.
[17] Finno RJ, Voss FT, Rossow E, Blackburn JT. Evaluating Damage Potential in Buildings Affected by Excavations. J Geotech Geoenviron 2005;131(10):1199–210.
[18] Negulescu C, Foerster E. Parametric studies and quantitative assessment of the vulnerability of a RC frame building exposed to differential settlements. Nat Hazards Earth Syst Sci 2010;10:1781–92. https://doi.org/10.5194/nhess-10-1781-2010.
[19] Fotopoulou S, Karafagka S, Pitilakis K. Vulnerability assessment of low-code reinforced concrete frame buildings subjected to liquefaction-induced differential displacements. Soil Dyn Earthquake Eng 2018;110:173–84. https://doi.org/10.1016/j.soildyn.2018.04.010.
[20] Gómez-Martínez F, Millen MDL, Alves Costa P, Romão X. Estimation of the potential relevance of differential settlements in earthquake-induced liquefaction damage assessment. Eng Struct 2020;211:110232. https://doi.org/10.1016/j.engstruct.2020.110232.
[21] Bao C, Ma X, Lim KS, Chen G, Xu F, Tan F, et al. Abd Hamide, Seismic fragility analysis of steel moment-resisting frame structure with differential settlement. Soil Dyn Earthquake Eng 2021;141:106526. https://doi.org/10.1016/j.soildyn.2020.106526.
[22] Miano A, Mele A, Calcaterra D, Martire DD, Infante D, Prota A, et al. The use of satellite data to support the structural health monitoring in areas affected by slow-moving landslides: a potential application to reinforced concrete buildings. Struct Health Monitor 2021;20(6):3265–87.
[23] Mele A, Miano A, Di Martire D, Infante D, Prota A, Ramondini M. Seismic assessment of an existing RC building affected by slow-moving landslides induced displacements monitored by remote sensing technique. In: Proc of the 8th ECCOMAS Thematic Conference on Comput Methods Struct Dyn Earthq Eng (COMPDYN), Athens, Greece, 27–30, June 2021.
[24] Di Carlo F, Miano A, Giannetti I, Mele A, Bonano M, Lanari R, et al. On the integration of multi-temporal synthetic aperture radar interferometry products and historical surveys data for buildings structural monitoring. J Civ Struct Health Monitor 2021;11(5):1429–47. https://doi.org/10.1007/s13349-021-00518-4.
[25] Drougkas A, Verstrynge E, Van Balen K, Shimoni M, Croonenborghs T, Hayen R, et al. Country-scale InSAR monitoring for settlement and uplift damage calculation in architectural heritage structures. Struct Health Monitor 2020; 1475921720942120. https://doi.org/10.1177/1475921720942120.
[26] Herrera G, Tomás R, Vicente F, Lopez-Sanchez JM, Mallorquí JJ, Mulas J. Mapping ground movements in open pit mining areas using differential SAR interferometry. Int J Rock Mech Min Sci 2010;47(7):1114–25.
[27] Giannico C, Ferretti A, Alberti S, Jurina L, Ricci M, Sciotti A. Application of satellite radar interferometry for structural damage assessment and monitoring LifeCycle and Sustainability of Civil Infrastructure Systems. In: 3rd International Symphosium on Life-Cycle Civil Engineering (IALCCE '12), Vienna, Austria, October 3-6, 2012.

[28] Talledo DA, Miano A, Bonano M, Di Carlo F, Lanari R, Manunta M, et al. Satellite radar interferometry: Potential and limitations for structural assessment and monitoring. J Build Eng 2022;46:103756. https://doi.org/10.1016/j.jobe.2021.103756.
[29] Nappo N, Peduto D, Polcari M, Livio F, Ferrario MF, Comerci V, et al. Subsidence in Como historic centre (northern Italy): Assessment of building vulnerability combining hydrogeological and stratigraphic features, Cosmo-SkyMed InSAR and damage data. Int J Disaster Risk Reduct 2021;56:102115. https://doi.org/10.1016/j.ijdrr.2021.102115.
[30] SAP2000 v21.0.2, Computers and Strucrures, Inc., 2019.
[31] Matlab. version 9.10.0.1602886 (R2021a). Natick, Massachusetts: The MathWorks Inc.; 2010.
[32] Di Domenico M, Ricci P, Verderame GM. Empirical calibration of hysteretic parameters for modelling the seismic response of reinforced concrete columns with plain bars. Eng Struct 2021;237:112120. https://doi.org/10.1016/j.engstruct.2021.112120.
[33] Panagiotakos TB, Fardis MN. Seismic response of infilled RC frames structures. Proceedings of the 11th world conference on earthquake engineering, Acapulco, México, 23-28 June 1996.
[34] Vamvatsikos D, Cornell CA. Incremental dynamic analysis. Earthq Eng Struct Dyn 2002;31(3):491–514.
[35] Vamvatsikos D, Cornell CA. Direct estimation of seismic demand and capacity of multi degree-of-freedom systems through incremental dynamic analysis of single degree of freedom approximation. J Struct Eng. 2005;131(4):589–99.
[36] Azarbakht A, Dolšek M. Progressive incremental dynamic analysis for first-mode dominated structures. J Struct Eng. 2011;137(3):445–55.
[37] Baraschino R, Baltzopoulos G, Iervolino I. R2R-EU: Software for fragility fitting and evaluation of estimation uncertainty in seismic risk analysis. Soil Dyn Earthquake Eng 2020;132:106093.
[38] DM 17/01/18 (2018) Norme tecniche per le costruzioni, Ministerial Decree (in italian).
[39] Eurocode 8, EN1998-3, Design of structures for earthquake resistance, Part 3: Assessment and retrofitting of buildings, CEN, Brussels, 2005.
[40] Jalayer F, Franchin P, Pinto PE. A scalar damage measure for seismic reliability analysis of RC frames. Earthq Eng Struct Dyn 2007;36(13):2059–79. https://doi.org/10.1002/eqe.704.
[41] Jalayer F, Ebrahimian H, Miano A. Intensity-based demand and capacity factor design: A visual format for safety checking. Earthquake Spectra 2020;36(4):1952–75.
[42] Miano A, Jalayer F, Ebrahimian H, Prota A. Cloud to IDA: Efficient fragility assessment with limited scaling. Earthquake Eng Struct Dyn 2018;47(5):1124–47.
[43] Helton JC, Davis FJ. Latin Hypercube Sampling and the propagation of uncertainty in analyses of complex systems. Reliab Eng Syst Saf 2003;81(1):23–69. https://doi.org/10.1016/S0951-8320(03)00058-9.
[44] Rubinstein RY. Simulation and the Monte Carlo method. New York: John Wiley and Sons; 1981.
[45] Olsson A, Sandberg G, Dahlblom O. On Latin hypercube sampling for structural reliability analysis. Struct Saf 2003;25(1):47–68.
[46] Stein M. Large sample properties of simulations using Latin hypercube sampling. Technometrics 1987;29(2):143–51.
[47] Ebrahimian H, De Risi R. Seismic reliability assessment, alternative methods for. *Encyclopedia of Earthquake Engineering* (book chapter). Editors: Michael Beer, Ioannis A. Kougioumtzoglou, Edoardo Patelli, Ivan Siu-Kui Au, Springer-Verlag Berlin Heidelberg, pp 2957-2981, 2014. DOI: 10.1007/978-3-642-36197-5_245-1. ISBN: 978-3-642-36197-5.
[48] Vamvatsikos D. Seismic performance uncertainty estimation via IDA with progressive accelerogram-wise latin hypercube sampling. J Struct Eng, 140; 2014. A4014015-1-10.
[49] Miano A, Jalayer F, Prota A. Considering structural modeling uncertainties using Bayesian cloud analysis. In: 6th ECCOMAS Thematic Conference on Computational Methods in Structural Dynamics and Earthquake Engineering (COMPDYN 2017), Rhodes Island, Greece, June 15-17, 2017.
[50] Vořechovský M, Novák D. Correlation control in small-sample Monte Carlo type simulations. I. A simulated annealing approach. Probab Eng Mech 2009;24(3):452–62.
[51] Eurocode 2, EN1992-1-1, Design of concrete structures: General rules and rules for buildings, CEN, Brussels, 2004.
[52] Circolare n. 7 C.S.LL.PP. 21 gennaio 2019 (2019), Commentary to NTC 2018 (in Italian).
[53] Eurocode 8, EN 1998-1, Design of structures for earthquake resistance, Part 1: General rules, seismic actions and rules for buildings, CEN, Brussels, 2003).
[54] Jalayer F, Ebrahimian H, Miano A, Manfredi G, Sezen H. Analytical fragility assessment using un-scaled ground motion records. Earth Eng Struct Dyn 2017;46(15):2639–63. https://doi.org/10.1002/eqe.2922.
[55] Legge n. 64 del 2 febbraio 1974, G.U. n. 76 del 21/03/1974 "Provvedimenti per le costruzioni con particolari prescrizioni perle zone sismiche" (in Italian).
[56] Ricci P, Manfredi V, Noto F, Terrenzi M, De Risi MT, Di Domenico M et al., RINTC-e: Towards seismic risk assessment of existing residential reinforced concrete buildings in Italy. In: Proceedings of the 7th ECCOMAS Thematic Conference on Computational Methods in Structural Dynamics and Earthquake Engineering, Crete, Greece, June 2019.
[57] R.D.L. 16 novembre 1939 n°2229 (Suppl. Ord. alla Gazz. Uff. del 18 aprile 1940 n°92) Norme per l'esecuzione delle opere in conglomerato cementizio semplice od armato, 1939 (in Italian).
[58] Al-Chaar G. Evaluating Strength and Stiffness of Unreinforced Masonry Infill Structures. Report, ERDC/CERL TR-02-1, January 2002.
[59] Verderame GM, Manfredi G, Frunzio G. Le proprietà meccaniche dei calcestruzzi impiegati nelle strutture in cemento armato realizzate negli anni '60. *X Convegno nazionale "L'Ingegneria Sismica in Italia"*, Potenza, Matera, September 9-13, 2001.
[60] Reluis, Stil v 1.0. (2019). Accessed at June 2021. Available at: http://www.reluis.it/index.php?option=com_content&view=article&id=199&Itemid=136&lang=it.
[61] Ricci P, Di Domenico M, Verderame GM. Experimental assessment of the in-plane/out-of-plane interaction in unreinforced masonry infill walls. Eng Struct 2018;173:960–78. https://doi.org/10.1016/j.engstruct.2018.07.033.
[62] Bal IE, Crowley H, Pinho R, Gulay FG. Structural characteristics of Turkish RC building stock in Northern Marmara region for loss assessment applications. ROSE research report no. 2007/03. IUSS Press; Pavia, Italy, 2007.
[63] Gaetani d'Aragona M, Polese M, Cosenza E, Prota A. Simplified assessment of maximum interstory drift for RC buildings with irregular infills distribution along the height. Bull Earthq Eng 2019;17(2):707–36.
[64] Borzi B, Pinho R, Crowley H. Simplified pushover-based vulnerability analysis for large-scale assessment of RC buildings. Eng Struct 2008;30(3):804–20.
[65] Hak S, Morandi P, Magenes G, Sullivan TJ. Damage control for clay masonry infills in the design of RC frame structures. J Earthquake Eng 2012;16(sup1):1–35.
[66] Deck O, Al Heib M, Homand F. Taking the soil-structure interaction into account in assessing the loading of a structure in a mining subsidence area. Eng. Struct. 2003;25(4):435–48.